The Plant Cell, Vol. 29: 2921–2939, November 2017, www.plantcell.org © 2017 The author(s).

Unexpected Connections between Humidity and Ion Transport Discovered Using a Model to Bridge Guard Cell-to-Leaf Scales

Yizhou Wang,[a,1,2] Adrian Hills,[a,1] Silvere Vialet-Chabrand,[b,1] Maria Papanatsiou,[a,1] Howard Griffiths,[c] Simon Rogers,[d] Tracy Lawson,[b] Virgilio L. Lew,[e] and Michael R. Blatt[a,3]

[a] Laboratory of Plant Physiology and Biophysics, University of Glasgow, Glasgow G12 8QQ, United Kingdom
[b] Biological Sciences, University of Essex, Colchester CO4 3SQ, United Kingdom
[c] Plant Sciences, University of Cambridge, Cambridge CB2 3EA, United Kingdom
[d] Computing Science, University of Glasgow, Glasgow G12 8QQ, United Kingdom
[e] Physiological Laboratory, University of Cambridge, Cambridge CB2 3EG, United Kingdom

ORCID IDs: 0000-0002-2188-383X (Y.W.); 0000-0002-4705-0756 (A.H.); 0000-0002-2105-2825 (S.V.-C.); 0000-0003-1871-9497 (M.P.); 0000-0003-3578-4477 (S.R.); 0000-0002-4073-7221 (T.L.); 0000-0002-0554-2701 (V.L.L.); 0000-0003-1361-4645 (M.R.B.)

Stomatal movements depend on the transport and metabolism of osmotic solutes that drive reversible changes in guard cell volume and turgor. These processes are defined by a deep knowledge of the identities of the key transporters and of their biophysical and regulatory properties, and have been modeled successfully with quantitative kinetic detail at the cellular level. Transpiration of the leaf and canopy, by contrast, is described by quasilinear, empirical relations for the inputs of atmospheric humidity, CO_2, and light, but without connection to guard cell mechanics. Until now, no framework has been available to bridge this gap and provide an understanding of their connections. Here, we introduce OnGuard2, a quantitative systems platform that utilizes the molecular mechanics of ion transport, metabolism, and signaling of the guard cell to define the water relations and transpiration of the leaf. We show that OnGuard2 faithfully reproduces the kinetics of stomatal conductance in *Arabidopsis thaliana* and its dependence on vapor pressure difference (VPD) and on water feed to the leaf. OnGuard2 also predicted with VPD unexpected alterations in K^+ channel activities and changes in stomatal conductance of the *slac1* Cl^- channel and *ost2* H^+-ATPase mutants, which we verified experimentally. OnGuard2 thus bridges the micro-macro divide, offering a powerful tool with which to explore the links between guard cell homeostasis, stomatal dynamics, and foliar transpiration.

INTRODUCTION

Stomata provide the main pathway for CO_2 entry for photosynthesis and for transpirational water loss across the leaf epidermis. Pairs of guard cells surround each stoma, regulating the aperture to balance the often conflicting demands for CO_2 and for water conservation. Guard cells open and close the pore, driven by osmotic solute uptake and loss, notably of K^+ and Cl^-, and by the synthesis and metabolism of organic solutes, especially sucrose (Suc) and malate (Mal) (Willmer and Fricker, 1996; Kim et al., 2010; Roelfsema and Hedrich, 2010; Lawson and Blatt, 2014; Jezek and Blatt, 2017). A number of well-defined signals, including light, CO_2, and the water stress hormone abscisic acid (ABA), modulate transport and solute accumulation to alter cell volume, turgor, and stomatal aperture. Much research at the cellular level has focused on these inputs and their connection to stomatal movements, especially stomatal closing. Studies have highlighted both Ca^{2+}-independent and Ca^{2+}-dependent signaling, including elevated free cytosolic Ca^{2+} concentration ($[Ca^{2+}]_i$), cytosolic pH (pH_i), protein kinases, and phosphatases, that inactivate inward-rectifying K^+ channels and activate Cl^- channels and outward-rectifying K^+ channels to bias the membrane for solute loss (Blatt et al., 1990; Lemtiri-Chlieh and MacRobbie, 1994; Grabov and Blatt, 1998, 1999; Marten et al., 2007; Assmann and Jegla, 2016; Jezek and Blatt, 2017).

At the tissue and whole-plant levels, by contrast, attention has been drawn to inputs closely tied to photosynthesis, including transpirational water loss (E) driven by the vapor pressure difference (VPD) between the atmosphere and the intercellular space of the leaf. Stomata respond to a drop in atmospheric humidity with a reduction in aperture (Lange et al., 1971; Buckley and Mott, 2002; Shope et al., 2008). This aperture change helps preserve water, albeit often at the expense of reduced carbon fixation (Lawson and Blatt, 2014). The immediate effect of reducing atmospheric humidity—that is, raising the VPD—is to increase the rate of transpiration driven by the difference in the vapor pressure of water between the inside and outside the leaf ($\Delta w = w_{leaf} - w_{air}$). The internal partial vapor pressure of water is almost always inferred and assumed to remain close to saturation, w_{sat} (Willmer and Fricker, 1996; Farquhar et al., 2001). For these reasons, stomatal conductance ($g_s = E/\Delta w$) is often plotted against external relative humidity ($RH = w_{air}/w_{sat}$).

[1] These authors contributed equally to this work.
[2] Current address: Department of Biology, Washington University, Saint Louis, MO 63130.
[3] Address correspondence to michael.blatt@glasgow.ac.uk.
The author responsible for distribution of materials integral to the findings presented in this article in accordance with the policy described in the Instructions for Authors (www.plantcell.org) is: Michael R. Blatt (michael.blatt@glasgow.ac.uk).

www.plantcell.org/cgi/doi/10.1105/tpc.17.00694

Despite the extensive body of phenomenological data, an understanding of the mechanism connecting stomatal transpiration with guard cell membrane transport is lacking. There is a clear need for a mechanistic framework that bridges the micro-macro gap between the guard cell and whole-plant transpiration. Here, we introduce such a framework, building on the original OnGuard platform that encompasses guard cell transport, signaling, and homeostasis and successfully models guard cells across species, including those of *Arabidopsis thaliana* (Chen et al., 2012; Hills et al., 2012; Wang et al., 2012). We show that this next-generation platform, OnGuard2, faithfully reproduces stomatal dependence on VPD and predicts emergent characteristics, including elevations in $[Ca^{2+}]_i$, unexpected alterations in the K^+ channel activities, and altered VPD responses in the *slac1* Cl^- channel and *ost2* H^+-ATPase mutants of Arabidopsis. We validate each of these predictions experimentally. The findings demonstrate that OnGuard2 provides a reliable representation of the mechanistic link between guard cell membrane transport and foliar transpiration.

RESULTS

Rationale for the Modeling Approach

The majority of mechanisms that have been proposed for the stomatal response to VPD assume that the response is caused by a change in foliar water potential or a parameter related to the rate of water vapor diffusion from the leaf. Although transpiration is affected by external w_{air} ($\Delta w = w_{leaf} - w_{air}$, often expressed as the corresponding difference in the mole fractions of water vapor), the vapor pressure of water in the leaf also depends on leaf temperature, T_{leaf}, which alters the equilibrium between the liquid and vapor phases of water. Leaf temperature affects other processes, however, notably photosynthesis and metabolism in the mesophyll (Smith and Dukes, 2013) and guard cells (Willmer and Fricker, 1996). Not surprisingly, most studies of foliar transpiration and stomatal response to VPD have employed changes in w_{air} at constant or near-constant T_{leaf}. In the natural environment, changes in temperature most often arise with solar radiation, the associated heat driving evaporation within the leaf which effectively absorbs the thermal load and facilitates transpiration to the surrounding air (Pieruschka et al., 2010). Thus, it is to be expected that, at a given air temperature, T_{leaf} will stabilize with near-constant irradiation, provided that water supply to the leaf is not limiting. As a first approximation, therefore, T_{leaf} is commonly assumed to be constant.

Beyond the drivers for evapotranspiration, most mechanistic models that have been proposed start from the premise either (1) that the guard cells respond to a chemical signal produced by evaporating site(s) distant from the guard cell (Buckley et al., 2003), or (2) that the guard cells are supplied by liquid flow through the epidermis and evaporation occurs directly from the guard cells (Farquhar, 1978; Maier-Maercker, 1983; Dewar, 1995; Buckley, 2005). The difficulty with the first model is that no obvious signal has been identified, beyond water in the vapor phase itself, that can account for key aspects of stomatal behavior, for example, the differential response of amphistomatous leaves to different VPDs on either side of the same leaf (Mott, 2007). The second model posits evaporation from the guard cells directly, leading to their water loss and stomatal closure. However, a growing body of evidence indicates that the bulk of the evaporation within the leaf occurs well away from the guard cells, dominated instead by evaporation from the vascular tissue, nearby mesophyll and pavement cells (Pieruschka et al., 2010; Rockwell et al., 2014; Buckley et al., 2017). These studies imply that water in the guard cell is maintained primarily by equilibration with water in the vapor phase within the adjacent substomatal cavity and the stomatal pore rather than by liquid flow through the cell wall and neighboring cells.

Regardless of their starting premise, virtually all models for transpiration to date have considered stomata to operate entirely on the basis of passive water flux driven by evaporation and diffusion without reference to solute transport in the guard cells and its consequences for osmotic water flux, turgor, and stomatal aperture. One exception is the hydromechanical model of Buckley, et al. (2003), which proposed a simple hyperbolic relation between the ATP concentration of the guard cells and their osmotic content. Even this model failed to incorporate guard cell solute transport explicitly, however, so obviating the intrinsic regulatory processes that are known to determine much of stomatal function (Jezek and Blatt, 2017). Furthermore, all mechanistic models to date have sought analytic solutions for endpoint or stationary states only. They therefore fail to address the wealth of information available relating to the temporal kinetics for stomatal movements and transpiration.

By contrast with analytical approaches, numerical computation allows flexibility in experimentally guided model design, and it is amenable to representing the temporal kinetics of interacting processes (Lew and Bookchin, 1986; Mauritz et al., 2009). It avoids solutions that may appear to provide simplified or explicit equations for a process but that sterilize the predictive power of model implementation. We previously used iterative numerical computation in developing the OnGuard platform to model membrane transport, signaling, and homeostasis in guard cells (Chen et al., 2012; Hills et al., 2012). OnGuard uses small increments in time to introduce deviations away from the previous steady state, calculating and logging the dynamic adjustments of ion flux, compartmental composition, membrane voltage, and guard cell volume that result with each step in time. It uses the sets of constants, nonlinear differential equations, and parameters contained within the model to calculate ion flux, while obeying the fundamental physical constraints of mass and charge conservation. It generates a new total solute content for the guard cell at the end of each time interval, using this value to calculate the new total and compartmental cell volumes and ion concentrations, the guard cell turgor, and stomatal aperture. Thus, like other computational approaches (Lew et al., 1979; Lew and Bookchin, 1986; Mauritz et al., 2009), OnGuard does not transit between two predefined states but, instead, begins from a starting, or reference, state (Chen et al., 2012; Hills et al., 2012), from which a new state evolves over each time increment.

Models resolved with this platform successfully recapitulated a wide range of known stomatal behaviors, including transport, diurnal changes in aperture, their dependencies on extracellular pH, KCl, and $CaCl_2$ concentrations (Chen et al., 2012), and oscillations in $[Ca^{2+}]_i$ and membrane voltage thought to facilitate stomatal closure (Blatt, 2000; McAinsh and Pittman, 2009; Minguet-Parramona et al., 2016). OnGuard models demonstrated true predictive power, for

example, in resolving the mechanisms behind the counterintuitive alterations in K^+ channel activity uncovered in the *slac1* Cl^- channel mutant of Arabidopsis, which we subsequently validated experimentally (Wang et al., 2012). Finally, OnGuard models provided a mechanistic understanding of $[Ca^{2+}]_i$ oscillation frequency and its relation to solute flux during stomatal closure (Minguet-Parramona et al., 2016).

OnGuard incorporates all the fundamental properties of the transporters at the plasma membrane and tonoplast that determine the osmotic relations of the guard cell, the salient features of Suc and Mal metabolism, and the essential H^+ and Ca^{2+} buffering characteristics that have been described in the literature (Hills et al., 2012; Jezek and Blatt, 2017). The OnGuard platform accommodates spectrally discrete irradiation, and it utilizes photosynthesis to energize membrane transport and Suc and Mal metabolism (Chen et al., 2012; Vialet-Chabrand et al., 2017). Within OnGuard, two key assumptions only are relevant to modeling evapotranspiration (we direct the reader to the detailed descriptions of Hills et al. [2012] and Chen et al. [2012]). These assumptions are that the water permeabilities of the plasma membrane and tonoplast are high, so water flux normally equilibrates rapidly with respect to ion transport, and that the apoplast of the cell wall space surrounding the guard cells provides a near-infinite reservoir for solutes uninfluenced by material entering or emanating from the guard cell. The first assumption is founded on reliable data (Hill and Findlay, 1981; Willmer and Fricker, 1996; Maurel, 1997; Chaumont and Tyerman, 2014; Maurel et al., 2015); it allows guard cell volume and turgor to be resolved from the Van't Hoff relation with stomatal aperture from empirical relations of steady state experimental measurements (Hills et al., 2012). The second assumption greatly simplifies a treatment of ion transport across the plasma membrane, leaving the external ion composition and the associated osmotic potential, C_{iso}, to be defined by the user. Although the platform does not account explicitly for ion exchange with the surrounding pavement cells, the latter assumption is consistent with the presumed role of the pavement cells in buffering apoplastic solutes transported by the guard cells and with the known and substantial cation buffer capacity of the cell wall matrix (Bowling, 1987; Bush and McColl, 1987; Marschner, 1995; Willmer and Fricker, 1996; Buckley et al., 2003).

These assumptions offer a starting point from which to accommodate stomatal responses to VPD, allowing us to develop the next-generation OnGuard2 platform from the core of knowledge subsumed within the original software. To bridge the gap from the microscopic physiology of solute transport in the guard cell to the macroscopic relations of foliar and whole-plant water flux, therefore, three key issues only need be addressed, namely, formalisms (1) that couple the guard cell to transpiration, (2) that account for water delivery to the leaf, and (3) that address water flux across the guard cell membrane. Below we summarize the reasoning and solutions behind each in turn. All the novel model developments are detailed in the Appendix at the end of this article together with Appendix Table 1 that summarizes the abbreviations for the various parameters and constants.

Connecting the Vapor Phase with Guard Cell Water

To accommodate evidence of evaporation away from the guard cells (Pieruschka et al., 2010; Rockwell et al., 2014; Buckley et al., 2017), we assume that water in the guard cell is maintained by equilibration with water in the vapor phase within the adjacent substomatal cavity and the stomatal pore. No system undergoing steady state flux can be fully at equilibrium, but it is an adequate approximation for evaporation, water vapor diffusion, and exchange inside a leaf. Like Peak and Mott (2011), we assume a constant leaf temperature, T_{leaf}, but provide both T_{leaf} and the air temperature, T_{air}, as parameters for runtime manipulation by the user, and we define a site, *p*, internal to the leaf and near the stomatal pore, with which guard cell water equilibrates (Figure 1). The advantage of this description is that it couples guard cell response to VPD through the vapor pressure of water at *p*, w_p. We stress that the *p* site concept does not imply a single, physical site with which guard cell water exchanges but represents a hypothetical position at a constant fraction of the resistance for water vapor diffusion to the outside (Peak and Mott, 2011). It implies a gradient in the vapor pressure of water between the sites of evaporation within the leaf and the outside, with the gradient extending through the stomatal pore and into the substomatal cavity. In other words, *p* defines a position along a standing gradient in water vapor that extends into the leaf air space.

In situ, much of the free (unoccluded) guard cell surface is exposed to the air within and immediately adjacent to the pore area between the guard cells. It follows that vapor exchange with the water in the guard cell will be subject to this gradient. We place *p* to the inside of the stomatal pore and interpret it to reflect the average of this vapor pressure gradient over the guard cell with which it exchanges. Similarly, we define this exchange to take place with the potential of liquid water averaged over the guard cell surface. Beyond exchange with the guard cell, the *p* concept does not specify the tissues from which the bulk of evaporation occurs and accommodates evaporation from the mesophyll as well as from the inner surface of the epidermis (Buckley et al., 2017). Since the conductivity for liquid water to the stomatal pore will be much lower than that for water vapor within the leaf air space, cells at different points in the leaf along the transpiration path will exchange with different partial pressures of water in the vapor phase.

It is important to note that Peak and Mott (2011) define the vapor phase equilibration of guard cell water without reference to the guard cell wall or its osmotic content. Thus, their original formulation cannot accommodate membrane transport between the apoplast and cytosol or water flux across the plasma membrane. Clearly, vapor exchange with liquid water of the guard cell must first occur between water in the guard cell wall and the air in the stomatal pore and substomatal cavity. We identify the external wall space as a compartment with a finite osmotic load, consistent with the vast literature of the past half-century on cell walls and the ionic relations of plant cells (compared with Findlay and Hope [1976], Taiz [1984], Bush and McColl [1987], Grignon and Sentenac [1991], Sanders et al. [2002], Holdaway-Clarke and Hepler [2003], and Jezek and Blatt [2017]). Thus, OnGuard2 incorporates the vapor phase at point *p* and its thermal equilibrium with the liquid phase water surrounding the guard cell so that the volume of the guard cell

$$V_T = Q_T/(P/RT + C_{iso}) \quad \text{where}$$
$$C_{iso} = C^o_{iso} + 1/v_L \cdot \ln\left(w_{sat}/w_p\right). \qquad (1a, b)$$

Hills et al. (2012) used Equation 1a in OnGuard, without reference to vapor phase equilibration, to describe the pressure-volume

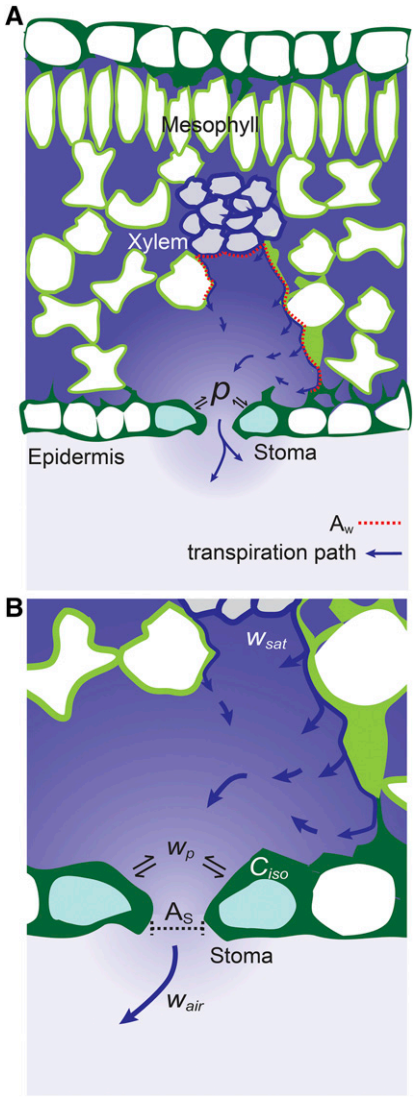

Figure 1. Schematic of Foliar Evapotranspiration from the Xylem through the Stomatal Pore (Stoma) and Point *p* Near the Inner Mouth of the Pore.

Full transection of the leaf is shown in **(A)** and an expanded schematic near the pore is shown in **(B)**. Liquid water from the xylem (gray cells, blue surface) feeds the surfaces of the surrounding mesophyll (green surfaces) and nearby pavement cells (dark green surfaces). The effective evaporative surface is indicated by the red dotted line (=A_w). Evaporation and vapor flux from this surface (blue arrows) maintain a high partial vapor pressure of water within the leaf and close to saturation (w_{sat}) adjacent this surface. As water vapor is lost through the stomatal pore (A_S indicated, defined by the width and breadth of the pore), driven by diffusion toward a lower w_{air}, a steady state gradient is established in the partial vapor pressure of water (background shaded blue color), reducing its value at w_p and at points toward the outside of the leaf. Mathematically, *p* represents the average of the water vapor gradient centered over the guard cell, which exchanges with liquid water in the guard cell wall, thereby affecting C_{iso}.

relations of the guard cell in relation to the total solute content of the guard cell, Q_T, and the apoplastic solute concentration, C_{iso}. Here, P is the turgor pressure, and R and T have their usual meanings. Rearranging Equation 1a and comparing it with Equation 4 of Peak and Mott (2011) yields the relation of Equation 1b, which effectively combines the osmotic potential of solutes in the cell wall with w_p and its equilibration with water in the wall (see Appendix). Here, v_L is the molar volume of water, and w_{sat} is the vapor pressure of water when saturated at T_{leaf}. We now define C^o_{iso} as the value of C_{iso} when $w_p = w_{sat}$. Thus, C^o_{iso} corresponds to the component of C_{iso} ascribed to solute in the cell wall, and the term $1/v_L \cdot \ln(w_{sat}/w_p)$ defines the component ascribed to vapor phase equilibration. Combining Equations 1a and 1b in OnGuard2 yields a simple formalism from which to calculate guard cell volume and turgor, and from these stomatal aperture, as functions both of extracellular osmotic solute and of the water vapor pressure w_p. Equation 1a,b thus is a critical step in bridging the micro-macro scales within OnGuard2.

Water Delivery to the Leaf and Water Vapor to p

Equation 1a,b has important implications for stomatal function. From the context of the guard cell, it equates the effects of depressing w_p within the leaf to those of adding osmotic solute to the cell wall. Furthermore, the very large value of $1/v_L$ (=56000 mmol/L) multiplies the natural logarithm of the ratio w_{sat}/w_p. So, even small increases in this ratio with a decline in w_p will have substantial effects on C_{iso}, thereby affecting guard cell volume, turgor pressure, and stomatal aperture. As w_p defines the water vapor pressure within the substomatal cavity adjacent to the guard cells, it also determines the rate of water loss from the leaf. From Fick's Law, the rate of water vapor diffusion through the stomatal pore is proportional to the driving force across the pore, $\Delta w_s = w_p - w_{air}$. A consideration of the diffusion pathway suggests that w_p normally will be close to w_{leaf} ($\approx w_{sat}$), which is often used as a convenient approximation to calculate stomatal conductance. However, depressing w_p when water delivery to the leaf is reduced will affect the rate of transpiration proportionally, all other factors being equal.

We resolve w_p assuming that water vapor lost via diffusion through the stomatal pore will be replaced by evaporation of water delivered to the leaf and diffusion to *p* (Figure 1). Thus, in the steady state, w_p can be sought through the balance between diffusion through the pore and delivery from the sites of evaporation (see Appendix). As noted above, evaporation within the leaf is a complex function of factors that include water delivery through the xylem, and its transfer across the evaporative surfaces of the surrounding mesophyll and nearby epidermal cells (Sack and Holbrook, 2006; Rockwell et al., 2014; Buckley et al., 2017). The evaporative surface area, A_W (Figure 1), is thought to vary substantially with hydraulic conductance through the xylem (Rockwell et al., 2014) as well as environmental factors, including w_{air} (Buckley et al., 2017). In OnGuard2, this factor becomes a user-defined parameter, the relative water feed (RWF), that encapsulates water delivery to the leaf, its conductance and evaporative distribution within the leaf, and, hence, any water stress arising through its restriction.

Water Flux across the Guard Cell Plasma Membrane

In operation, OnGuard2 calculates and logs the dynamics of changes in flux, compartmental composition, membrane voltage, and all other variables using sets of nonlinear differential equations

while obeying the fundamental physical constraints of mass and charge conservation. With each small step in time, the routine resolves a new pseudo-steady state that satisfies these physical constraints in relation to flux. The approach is common to modeling strategies that use iterative numerical calculation to integrate the temporal kinetics of a complex network of processes, but it generally imposes a practical constraint on model construction: By establishing a new steady state within each time interval, it presents a barrier to any temporal dynamics that might be encoded separate to the iteration cycle.

In the original OnGuard platform, we resolved guard cell volume, turgor, and stomatal aperture from the change in Q_T using the Van't Hoff relation assuming that the water permeabilities of the plasma membrane and tonoplast are high. In other words, water permeability across the guard cell membrane was assumed not to limit V_T. There are situations, however, in which water flux is slowed (Shope et al., 2008; Prado et al., 2013; Chaumont and Tyerman, 2014). Indeed, there is good evidence to suggest that the bulk of water flux is mediated by aquaporins at the plasma membrane and their activity is vital for stomatal movements in the intact leaf (Yang et al., 2006a, 2006b; Grondin et al., 2015). Thus, a treatment of stomatal transpiration must also provide for water flux and its regulation across the guard cell plasma membrane.

Within any series of iterative time increments, it is possible to generate a secondary relaxation over multiple increments by interleaving a time-dependent alteration to the incremental change in the process output without imposing internal complexity to the computational cycle. To a first approximation, water flux will follow a change in osmotic potential across the membrane with a simple exponential relaxation to a new steady state (Murai-Hatano and Kuwagata, 2007; Chaumont and Tyerman, 2014; Maurel et al., 2015). Therefore, to enable independent control of water flux in OnGuard2 consistent with a reduced osmotic permeability, we assigned water flux to a population of aquaporins with an exponential pseudo-rate constant, *f*, to adjust the increment in cell volume with each iteration (see Appendix). We add the adjusted volume increment to the previous cell volume and then calculate the new cytosolic and vacuolar volumes, solute concentrations and turgor pressure. Thus, *f* serves as a factor, related to membrane water permeability, that defines the relaxation in water flux relative to water equilibration with ion transport. In so doing, water flux remains an output of modeling.

Finally, we implemented ligand sensitivity to *f* (see Appendix), much as previously described for ion transport (Hills et al., 2012). There is a general consensus that the activity of plasma membrane aquaporins, and osmotic permeability generally, is suppressed only as cytosolic pH approaches a value of 7.0 and below (Tournaire-Roux et al., 2003; Verdoucq et al., 2008; Bellati et al., 2010; Maurel et al., 2015). However, quantitative information relevant to aquaporin regulation by $[Ca^{2+}]_i$ is scant and quantitatively conflicted although, again, there is general agreement that elevated $[Ca^{2+}]_i$ inhibits aquaporin activity. We incorporated ligand sensitivities for cytosolic $[H^+]$ and $[Ca^{2+}]_i$ with a K_H of 0.16 μM and a K_{Ca} of 0.4 μM, the latter representing a midpoint within the range of values currently reported for aquaporins from the plant plasma membrane (Alleva et al., 2006; Verdoucq et al., 2008) (Supplemental Appendix 1).

OnGuard2 Predicts a Steep Dependence of g_s at Limiting Hydraulic Feed

OnGuard2 predicted changes in stomatal aperture and g_s that faithfully reproduced experimental measurements across a wide range of conditions in water feed and VPD (Figure 2). The model also demonstrated a dependence on temperature (Supplemental Figure 1) that is broadly consistent with the curvilinear relationships previously reported for stomatal aperture across a number of species (Wilson, 1948; Stalfelt, 1962; Spence et al., 1984; Willmer and Fricker, 1996; Urban et al., 2017). Step increases in VPD (decreasing %RH outside) reduced steady state turgor, aperture, and g_s with a concurrent increase in total guard cell osmolarity; these values reversed when VPD was returned to its starting value. With RWF set to 100, equivalent to a well-watered plant, simulations showed a shallow dependence on VPD in aperture and g_s, even when the vapor content of the air outside the leaf was reduced to 10% RH. When RWF of the leaf was reduced, notably below 40, the sensitivity to VPD was strongly enhanced (Figures 2A and 2C) much like g_s from Arabidopsis with decreasing soil water content (Figures 2B and 2C). That g_s is weakly dependent on VPD unless water availability is limiting (Willmer and Fricker, 1996; Caldeira et al., 2014; Locke and Ort, 2015) is therefore faithfully reported in the model outputs.

Analysis of these outputs during VPD steps explains the detailed mechanism behind the stomatal response. Declining apertures were accompanied by increases in osmotic solute concentrations that arose from the loss of water from the guard cells and their decrease in volume. K^+ concentration rose in proportion with the decrease in cell volume in both the vacuole and cytosol (Figure 3A), and both remained elevated during the step change in VPD, as expected. Mal also rose throughout this period (Figure 3B), accompanied by a pH_i-associated stimulation in Mal synthesis (Supplemental Figure 2). However, after an initial rise, cytosolic and vacuolar Cl^- declined to roughly the concentrations expected without the VPD step (Figure 3C). Thus, with elevated VPD the model predicted a preference for Mal retention over Cl^- as a counterion, consistent with past evidence for enhanced Mal synthesis and accumulation with osmotic stress (Asai et al., 1999, 2000).

The simulations with VPD were also marked by a rise in $[Ca^{2+}]_i$, and its oscillation together with plasma membrane voltage (Figures 3D and 3E), until a new steady state was achieved. These rapid oscillations have been associated with stomatal closure and, like slower oscillations in simulation and in vivo, are thought to facilitate solute efflux during the depolarized phase of each oscillatory cycle (Grabov and Blatt, 1998; Minguet-Parramona et al., 2016). The elevated $[Ca^{2+}]_i$ resulted from an increase in vacuolar Ca^{2+} concentration and driving force for Ca^{2+} influx across the tonoplast (Supplemental Figure 2). Elevated $[Ca^{2+}]_i$ promoted the efflux of K^+ and Cl^- during depolarizations; K^+ and Mal efflux was compensated for by K^+ uptake via H^+-coupled K^+ transport and by enhanced Mal synthesis arising from the mass action of the increased sugar substrate concentration and the alkaline shift in pH_i.

Counterintuitive Alterations in K^+ Channel Activities

In simulation, increasing VPD enhanced the outward-rectifying ($I_{K,out}$) and reduced the inward-rectifying ($I_{K,in}$) K^+ channel currents (Figures

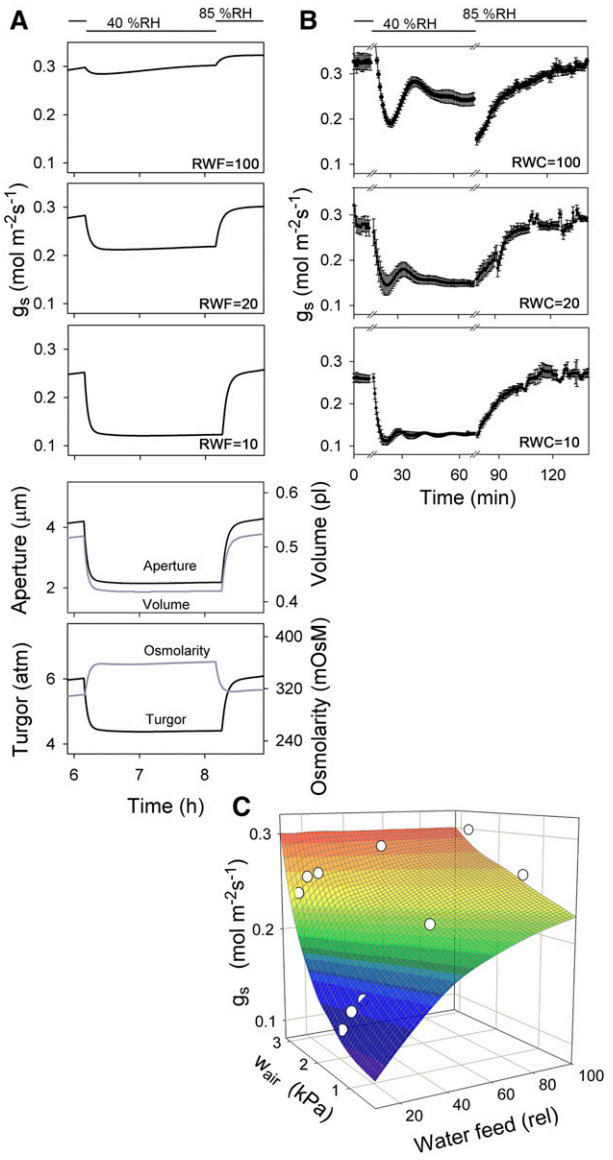

Figure 2. OnGuard2 Reproduces Stomatal Conductance (g_s) and Its Dependence on the Partial Vapor Pressure of Water in the Air (w_{air}) and RWF Available for Transpiration from the Plant.

(A) Model outputs for g_s with VPD steps generated with steps from 85%RH to 40%RH, and with RWF values of 100, 20, and 10, as indicated. Model outputs for aperture, guard cell volume, turgor, and osmolarity (bottom two graphs) correspond to g_s with RWF = 10.

(B) g_s from wild-type Arabidopsis with steps from 85%RH to 40%RH ($n \geq 3$ independent experiments in each case). Transients during the first 10 min omitted for clarity. Damped oscillations at higher relative water content (RWC) of the soil are probably associated with the Ivanoff effect and subsequent changes in turgor of the surrounding epidermal cells (Lawson and Blatt, 2014).

(C) Steady state dependence of g_s on w_{air} and RWF determined from the OnGuard2 model (surface plot, includes data in **[A]**) overlaid with experimental measurements (open symbols) from Arabidopsis, including the data in **(B)**, plotting RWC as a percentage of saturation (=100). Note that a direct relationship between RWF and RWC is not implied, although water feed to the leaf will depend on water available in the soil.

4A and 4B). The rise in $I_{K,out}$ is consistent with the mass action effect of the increased cytosolic K^+ concentration and stimulation of the current with elevated pH_i; the reduced $I_{K,in}$ arises from elevated $[Ca^{2+}]_i$ (Grabov and Blatt, 1999; Chen et al., 2012; Minguet-Parramona et al., 2016). These changes bias the membrane for stomatal closure. Returning VPD to its starting value yielded an unexpected hysteresis and overshoots in several outputs, predictions amenable to experimental testing. Notably, $I_{K,in}$ rose substantially over the control before the VPD step (Figure 4B)—an effect ascribed to reduced $[Ca^{2+}]_i$ (Figure 3D) that relieved the partial inhibition of the K^+ channel (Grabov and Blatt, 1999; Chen et al., 2012)—despite the recovery in turgor and aperture (Figure 2).

To test this counterintuitive prediction, we recorded K^+ currents under voltage clamp while challenging guard cells in epidermal strips with mannitol and polyethylene glycol 4000 to provide step changes of external osmolality equivalent to VPD changes. As noted above, OnGuard2 couples transport with external osmotic potential, whether as a consequence of a change in VPD or external osmotic solute content. From Equation 1b, adding 300 mOsM solute in C_{iso} is equivalent to a decrease of 0.6%RH at *p*, that is adjacent to the guard cells in the intercellular air space of the leaf (Figure 1), when external humidity is 40%RH (Figures 2A

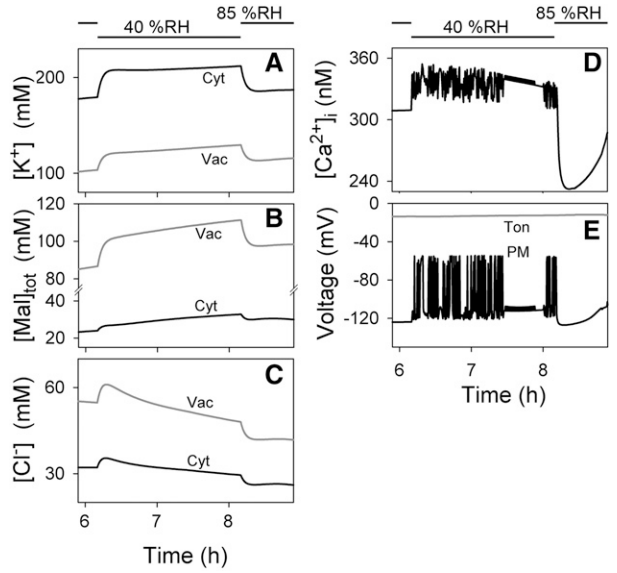

Figure 3. The OnGuard2 Model of Wild-Type Arabidopsis Predicts a Preferential Accumulation of Total Mal over Cl^-, Elevated Cytosolic Free $[Ca^{2+}]$ ($[Ca^{2+}]_i$) in the Face of an Increase in VPD, and a Substantial Undershoot in $[Ca^{2+}]_i$ on Its Recovery.

OnGuard2 outputs for VPD steps generated by varying external humidity between 85%RH and 40%RH with a relative water feed of 10. Plotted are cytosolic and vacuolar $[K^+]$ **(A)**, total [Mal] **(B)**, $[Cl^-]$ **(C)**, $[Ca^{2+}]_i$ **(D)**, and plasma membrane and tonoplast voltage **(E)**. Corresponding outputs for g_s, stomatal aperture, turgor, and osmolarity are shown in Figure 2A. Additional OnGuard2 outputs are summarized in Supplemental Figure 2. Oscillations in $[Ca^{2+}]_i$ and plasma membrane voltage, and associated oscillations in other flux outputs (Supplemental Figure 2) are associated with the decline in stomatal aperture (Minguet-Parramona et al., 2016). These oscillations are primarily associated with the substantial osmotic flux during stomatal closing.

and 2C). As predicted, we found (Figures 4C and 4D) that a 300 mOsM rise outside led to a rapid and prolonged reduction in $I_{K,in}$ and an increase in $I_{K,out}$. Washing out the osmotica led to a recovery in $I_{K,out}$. Significantly, washout was also accompanied by a large overshoot in $I_{K,in}$ that remained elevated for 5 to 10 min before declining toward the initial current characteristics.

We analyzed the steady state K^+ currents using a Boltzmann equation of the form

$$I = g_{max} \cdot (V\text{-}E_K) \Big/ \left(1 + e^{\delta F(V\text{-}V_{1/2})/RT}\right) \quad (2)$$

where g_{max} is the maximum ensemble conductance, V is the voltage, $V_{1/2}$ is the voltage at which $g = 0.5 \cdot g_{max}$, δ is the voltage sensitivity coefficient of the channel, E_K is the equilibrium voltage for K^+, and F is the Faraday constant. Analysis of $I_{K,in}$ showed that adding and removing osmolyte evoked shifts in $V_{1/2}$ of -12 ± 4 mV and +9 ± 3 mV, and altered g_{max} by $-40 \pm 3\%$ and $+73 \pm 5\%$, respectively, relative to the initial values (Figure 4E), as expected for $[Ca^{2+}]_i$ ranging over roughly 200 to 400 nM (Grabov and Blatt, 1999; Wang et al., 2012). The same manipulations affected $I_{K,out}$, but in a manner consistent with the reversible changes in pH_i and $[K^+]_i$ with cell volume (Figure 4F). The timescales of these recordings, typically 20 to 30 min, precluded measurements to full recovery. However, the reversible increase in $I_{K,out}$ with osmotic strength and the counterintuitive enhancement in $I_{K,in}$ on its washout validate the model predictions. We also tested the rise in $[K^+]_i$ on adding 300 mOsM solute using tail currents of the K^+ channels to quantify the change in the equilibrium voltage for K^+ (Blatt and Clint, 1989). The analysis indicated a small but significant displacement of -4 ± 1 mV (n = 24), indicating roughly a 30 mM increase in $[K^+]_i$ with the osmotic challenge and again consistent with the modeling.

OnGuard2 Predicts Altered VPD Responses in the slac1 and ost2 Mutants

The *ost2* mutation affects the predominant H^+-ATPase, AHA1 in Arabidopsis guard cells. It renders the H^+-ATPase largely insensitive to Ca^{2+} and leads to membrane hyperpolarizations with stomata of the *ost2* mutant responding poorly to ABA and light-dark transitions (Merlot et al., 2007). An intuitive assessment, however, might suggest little effect of external osmotica or VPD changes on the K^+ channels (Assmann et al., 2000; McAdam and Brodribb, 2016). We modeled the *ost2* mutant by eliminating H^+-ATPase sensitivity to $[Ca^{2+}]_i$, as was our previous strategy to model the reduced response to light-dark transitions of the *ost2* mutant (Blatt et al., 2014). As expected, the *ost2* model showed elevated $[Ca^{2+}]_i$ and pH_i as well as a hyperpolarization of the plasma membrane, even in the absence of a VPD challenge (Figure 5). The rise in $[Ca^{2+}]_i$ can be seen as a direct result of uncoupling the H^+-ATPase from $[Ca^{2+}]_i$ regulation, its hyperpolarization of the membrane (Supplemental Figure 3), and the increased driving force for Ca^{2+} entry across the membrane. The rise in pH_i, likewise, can be seen to arise from uncoupling $[Ca^{2+}]_i$ control of the H^+-ATPase, thereby facilitating H^+ transport out of the guard cell (Supplemental Figure 3). In turn, the *ost2* model predicted a strong suppression of $I_{K,in}$ and enhancement of $I_{K,out}$ even in the absence of a VPD step, both effects the direct consequences of the elevated $[Ca^{2+}]_i$ and pH_i (Figure 5).

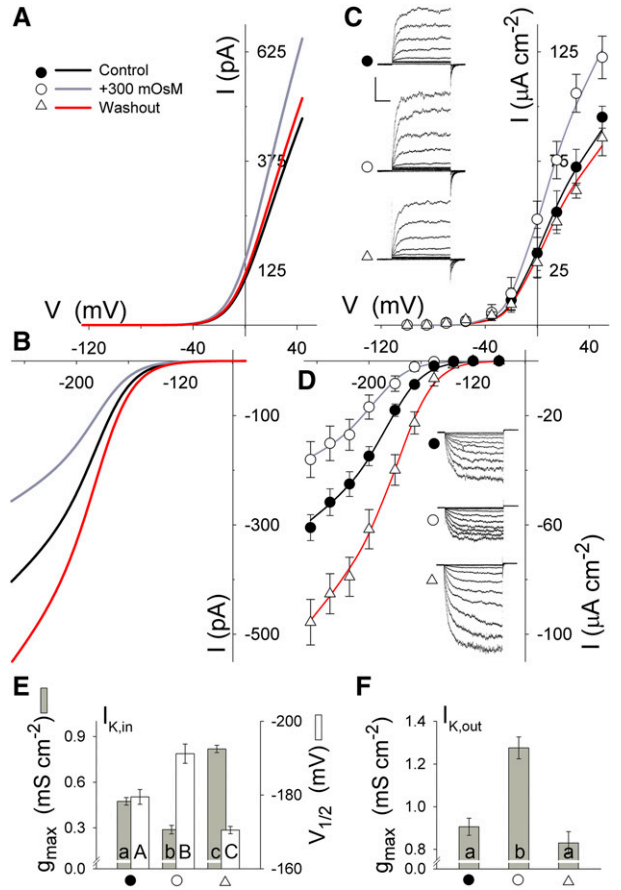

Figure 4. OnGuard2 Accurately Predicts Alterations in K^+ Channel Activities with Step Changes in VPD That Are Validated Experimentally with Equivalent Changes in External Osmolarity.

(A) and **(B)** OnGuard2 outputs for the outward-rectifying ($I_{K,out}$; **[A]**) and inward-rectifying K^+ current ($I_{K,in}$; **[B]**) before, 10 min into a VPD step with 40%RH (= +300 mOsM), and 5 min after recovery (washout). Outputs correspond to the data of Figure 2A with RWF = 10.

(C) and **(D)** Voltage clamp measurements from wild-type Arabidopsis guard cells before, during challenge with 300 mOsM mannitol, and 5 min after mannitol washout. Voltage stepped from a holding potential of −100 mV in 10 steps from −100 mV to +50 mV **(C)** for $I_{K,out}$ and to −250 mV **(D)** for $I_{K,in}$. Data are means ± SE (n = 9). Curves are nonlinear least-squares fittings performed jointly for each current to Equation 2. Fittings yielded common voltage-sensitivity coefficients (δ) of 1.78 ± 0.07 and 1.94 ± 0.13 for $I_{K,in}$ and $I_{K,out}$, respectively, and a common midpoint voltage ($V_{1/2}$) for $I_{K,out}$ of −7 ± 2 mV (see also Supplemental Table 2). Insets: Current traces from one guard cell, cross-referenced by symbol. Scale: 200 pA ($I_{K,out}$) and 150 pA ($I_{K,in}$) vertical, 1 s horizontal. Note the suppressed $I_{K,in}$ in mannitol and its overshoot on mannitol washout that are predicted outcomes of its dependence on $[Ca^{2+}]_i$ (Grabov and Blatt, 1999; Wang et al., 2012).

(E) Ensemble conductance (g_{max}) and $V_{1/2}$ for $I_{K,in}$ **(D)**, determined by fitting as indicated above and cross-referenced by symbol. Letters indicate significant differences ($P < 0.001$).

(F) Ensemble conductance (g_{max}) for $I_{K,out}$ **(C)**, determined by fitting as indicated above cross-referenced by symbol. Letters indicate significant differences ($P < 0.001$).

Unexpectedly, the *ost2* model showed slowed kinetics in g_s and aperture with step changes in VPD, greatly reduced $I_{K,in}$, and enhanced $I_{K,out}$, with the VPD sensitivities of both K^+ currents suppressed (Figures 5A to 5C). The model output (Supplemental Figure 3) showed that these effects could be attributed foremost to the elevated pH_i and $[Ca^{2+}]_i$ (Figure 5D) driven by the Ca^{2+}-insensitive H^+-ATPase, thereby maintaining the more alkaline pH_i, polarizing plasma membrane to prevent voltage-dependent activation of SLAC and R-type (ALMT) anion channels, and suppressing solute and water efflux from the guard cells.

To test these predictions, we performed gas exchange measurements on leaves, recorded K^+ currents under voltage clamp, and measured $[Ca^{2+}]_i$ and pH_i in vivo following injections of the Ca^{2+}- and H^+-sensitive dyes Fura2 and BCECF, respectively (Grabov and Blatt, 1998, 1999; Wang et al., 2012). As predicted, the *ost2* mutant showed greatly slowed stomatal kinetics in response to step increases in VPD and its recovery (Figures 6A and 6B). Furthermore, the *ost2* mutant also showed a reduced $I_{K,in}$, elevated $I_{K,out}$, and a suppressed response of the currents to external osmolarity (Figures 6C and 6D), as predicted by the *ost2* model in OnGuard2.

Recording $[Ca^{2+}]_i$ and pH_i showed modest elevations with a 300 mOsM rise outside in guard cells of wild-type Arabidopsis (Figure 6F). There are no precedents for measurements of $[Ca^{2+}]_i$ and pH_i in guard cells under osmotic challenge. However, the background data taken prior to osmotic challenge are similar to recordings from guard cells of a number of species including Arabidopsis (Jezek and Blatt, 2017), and the measurements following 300 mOsM steps are consistent with $[Ca^{2+}]_i$ recorded under similar conditions from other Arabidopsis tissues (Yuan et al., 2014). Guard cells of the *ost2* mutant showed a substantial elevation in background $[Ca^{2+}]_i$ and pH_i and a further rise in $[Ca^{2+}]_i$ with the osmotic step (Figures 6E and 6F), as predicted by the modeling. Significantly, both the background $[Ca^{2+}]_i$ and pH_i in the *ost2* mutant were substantially above the apparent K_{Ca} for inhibition of $I_{K,in}$ and below the K_H for inhibition of $I_{K,out}$, respectively (Grabov and Blatt, 1997, 1999; Jezek and Blatt, 2017), consistent with the relative suppression in the responses of both currents to the osmotic step. We found no evidence for a change in channel expression in the *ost2* mutant (Supplemental Figure 4). The findings therefore validate the predicted, but unexpected, connection between the H^+-ATPase and capacity for K^+ flux through the dominant guard cell K^+ channels, which are linked through the $[Ca^{2+}]_i$ and pH_i intermediates in vivo.

Finally, we examined stomatal closing and its recovery with step changes in VPD in the *slac1* null mutant. Previous work with the original OnGuard platform uncovered counterintuitive predictions that nonetheless proved valid on experimental analysis, including an unexpected connection between the SLAC1 anion channel, required for stomatal closing, and the kinetics of K^+ uptake during stomatal opening (Wang et al., 2012). These effects were demonstrated to arise from an increase in pH_i buffering and a substantial increase in background $[Ca^{2+}]_i$ in the *slac1* mutant, both effects leading to an overall suppression in $I_{K,in}$ and enhancement in $I_{K,out}$. Indeed, at the cellular level, the *slac1* model, in which the SLAC current was eliminated, yielded elevated stomatal apertures with increased osmotic content and turgor (Wang et al., 2012), but the implications for

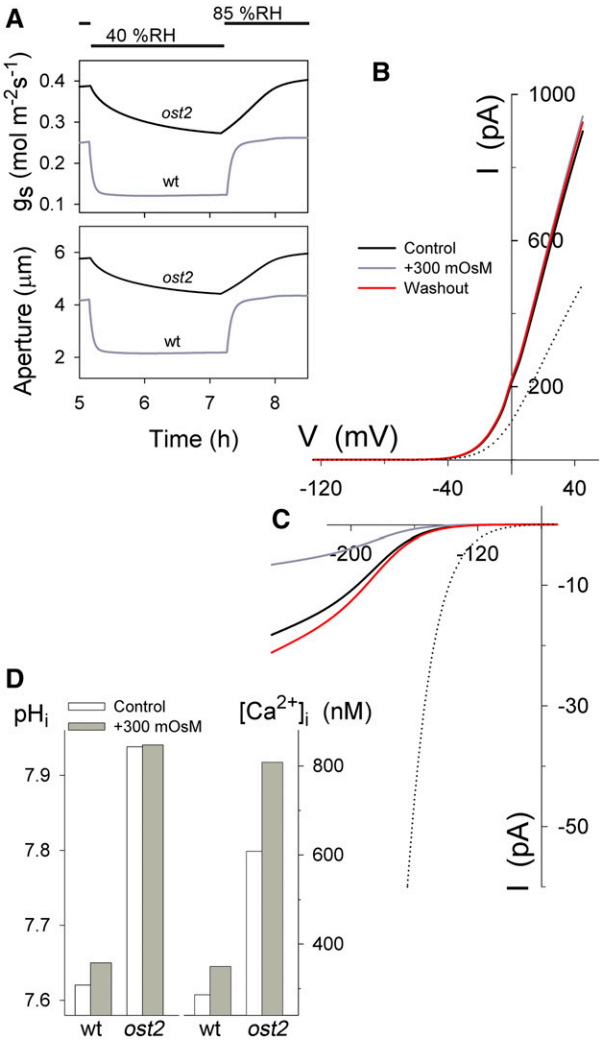

Figure 5. The OnGuard2 Model for the *ost2* Mutation Predicts Slowed Kinetics in g_s and Aperture with Step Changes in VPD and reduced Alterations in K^+ Channel Activities with Equivalent Step Changes in External Osmolarity Compared with the Wild Type.

(A) OnGuard2 outputs in g_s and stomatal aperture for the *ost2* and wild-type models with external %RH as indicated.
(B) and **(C)** OnGuard2 outputs of the *ost2* model for the outward-rectifying ($I_{K,out}$; **[B]**) and inward-rectifying K^+ current ($I_{K,in}$; **[C]**) before, 10 min into a step to 40%RH (= +300 mOsM), and 5 min after its recovery (red, washout), as in Figures 4A and 4B. Dotted curves included from the wild-type controls in Figures 4A and 4B for reference. Note the substantially enhanced $I_{K,out}$ and reduced $I_{K,in}$ in *ost2* compared with the wild type, predicted as a consequence of the elevated $[Ca^{2+}]_i$ and pH_i.
(D) OnGuard2 outputs for cytosolic-free $[Ca^{2+}]_i$ ($[Ca^{2+}]_i$) and pH (pH_i) before and during VPD (osmotic) steps from the wild-type and *ost2* models. Note the elevated pH_i and $[Ca^{2+}]_i$ of the *ost2* model, the latter further enhanced on VPD (osmotic) challenge.

VPD-dependent transport and g_s remained unresolved in the absence of a mathematical connection to the whole leaf.

We introduced the same step changes in VPD with the *slac1* model (Wang et al., 2012) using OnGuard2 to examine the consequences for transpiration. The results uncovered both macroscopic effects

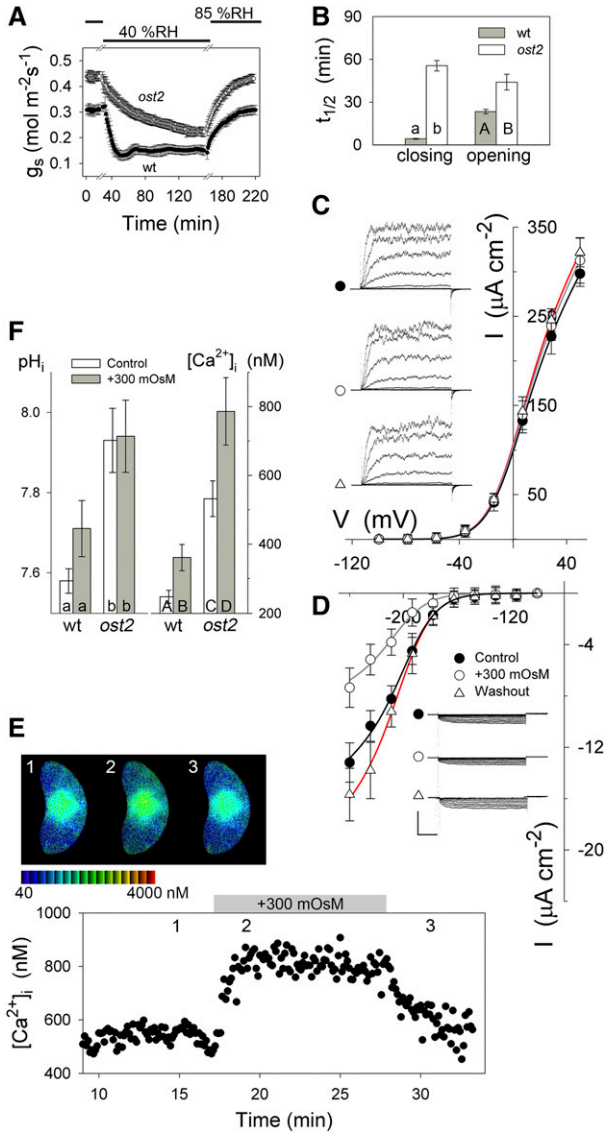

Figure 6. The *ost2* Mutation Elevates g_s, Slows Its Response to Step Changes in VPD, and Suppresses the Inward-Rectifying K^+ Current and Its Overshoot with Equivalent Changes in External Osmolarity.

(A) g_s recorded from the *ost2* mutant wit steps from 85 to 45%RH (above). Data are means ± SE of four independent experiments. Parallel data from wild-type Arabidopsis included for comparison. Transients during the first 10 min omitted for clarity.

(B) Analysis of halftimes ($t_{1/2}$) for g_s relaxations on closing and opening in **(A)**. Note the increases in $t_{1/2}$ for closure and reopening, as predicted. Significant differences indicated by lettering ($P < 0.05$).

(C) and **(D)** Voltage clamp measurements from guard cells of the *ost2* mutant before, during challenge with 300 mOsM mannitol, and 5 min after mannitol washout (red curves). Voltage stepped from a holding potential of −100 mV in 8 steps from −100 mV to +50 mV **(C)** for $I_{K,out}$ and in 10 steps to −250 mV **(D)** for $I_{K,in}$. Data are means ± SE ($n = 5$). Curves are nonlinear least-squares fittings performed jointly for each current to Equation 2. Fittings yielded common voltage sensitivity coefficients (δ) of 1.83 ± 0.09 and 1.87 ± 0.04 for $I_{K,in}$ and $I_{K,out}$, respectively, and a common midpoint voltage ($V_{1/2}$) for $I_{K,out}$ of −3 ± 2 mV (see also Supplemental Table 2). Insets: Current traces from one guard cell, cross-referenced by symbol. Scale: 500 pA ($I_{K,out}$) and 150 pA ($I_{K,in}$) vertical, 1 s horizontal. Note the expanded current scale in **(D)** showing the suppressed $I_{K,in}$ in mannitol and the absence of a significant overshoot on its washout, as predicted.

(E) and **(F)** Cytosolic-free $[Ca^{2+}]$ ($[Ca^{2+}]_i$) and pH (pH_i) recorded from wild-type and *ost2* mutant guard cells before and during challenge with 300 mOsM mannitol. $[Ca^{2+}]_i$ and pH_i recorded by ratiometric imaging with fluorescent dyes Fura2 and BCECF, respectively. Representative $[Ca^{2+}]_i$ recordings, pseudocolor scale, and time course for the *ost2* mutant are shown in **(E)** with time points of the images shown indicated by numbers (1, 2, and 3). Data in **(F)** are means ± SE ($n \geq 4$) with the average $[Ca^{2+}]_i$ determined from a 1-μm (4 pixel depth) band around the cell periphery. Significant differences are indicated by lettering ($P < 0.05$).

on g_s as well as microscopic changes in channel current. Significantly, at the macroscopic level, OnGuard2 returned four outputs mirroring the response in stomatal aperture: an elevated g_s, a larger change in g_s with VPD, its slowed rate of decline, and its accelerated recovery on returning VPD to the starting value (Figure 7A). All four predictions were confirmed experimentally (Figure 7B), the first two also noted before (Merilo et al., 2013). Of interest, OnGuard2 correctly predicted the accelerated recovery in aperture and g_s in the *slac1* mutant when compared with the guard cells of the wild type. This finding contrasts with the slower opening of the *slac1* mutant modeled and observed in response to light (Wang et al., 2012) and highlights the difference in mechanics and response associated with the two stimuli. The *slac1* model yielded two further sets of microscopic outputs also not foreseen previously, predictions that could only be drawn from quantitative systems modeling across the micro-macro scales (Figures 7C and 7D). (1) The *slac1* model returned a much reduced current decline and overshoot in $I_{K,in}$ on VPD recovery. (2) It predicted an increased background and virtual loss in sensitivity of $I_{K,out}$ to changes in VPD.

We tested these predictions, experimentally challenging guard cells of wild-type, *slac1*, and the *SLAC1*-complemented *slac1* line (Wang et al., 2012) to step changes in external osmotic strength as before while recording the K^+ currents under voltage clamp. Results with the *slac1* mutant (Figures 7E and 7F) confirmed both predictions, while *SLAC1*-complemented *slac1* Arabidopsis yielded currents indistinguishable from those of the wild type (Figure 4) (Wang et al., 2012). The findings underline the importance of anion efflux through SLAC1 for VPD-associated stomatal responses and its association with the K^+ channels. Most important, however, together with the analysis of the *ost2* mutant, they demonstrate the predictive power of OnGuard2 and its ability to bridge the micro-macro gap in stomatal transpiration and its response to VPD.

DISCUSSION

Stomatal aperture and conductance are affected by the vapor pressure difference between inside and outside the leaf, especially when water delivery to the leaf is limiting (Lange et al., 1971; Willmer and Fricker, 1996; Pieruschka et al., 2010). Although widely recognized, previous efforts failed to explain the mechanistic connection to the microscopic processes of guard cell ion

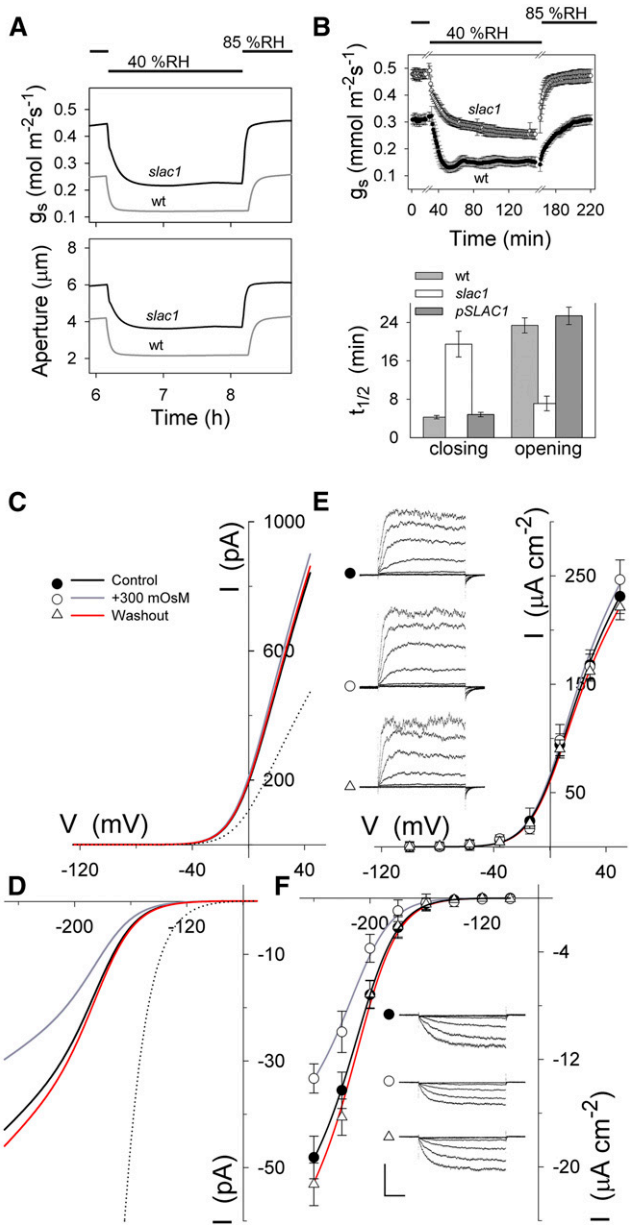

Figure 7. The OnGuard2 Model for the Arabidopsis *slac1* Mutation Accurately Predicts Alterations in Stomatal Conductance (g_s) and Its Kinetics with Step Changes in VPD and Alterations in K^+ Channel Activities with Equivalent Step Changes in External Osmolarity.

(A) OnGuard2 outputs in g_s and stomatal aperture for the *slac1* model with VPD on steps in external %RH.

(B) g_s recorded from wild-type, *slac1* mutant, and *ProSLAC1:SLAC1* complemented *slac1* mutant (*pSLAC1*) Arabidopsis with VPD on steps in external %RH (above). Analysis of halftimes ($t_{1/2}$) for g_s relaxations on closing and opening (below). Data are means ± SE of six independent experiments. Transients during the first 10 min with steps in %RH omitted for clarity. Note the significant increase in $t_{1/2}$ for closure and decrease in $t_{1/2}$ for reopening, as predicted from the modeling.

(C) and **(D)** OnGuard2 outputs of the *slac1* model for the outward-rectifying ($I_{K,out}$; **[C]**) and inward-rectifying K^+ current ($I_{K,in}$; **[D]**) before, 10 min into a VPD step with 40%RH (= +300 mOsM), and 5 min after its recovery (red, washout), as in Figure 4. Dotted curves included from the wild-type controls in Figures 4A and 4B for reference. Note the substantially enhanced $I_{K,out}$ and reduced $I_{K,in}$ compared with the wild type, predicted as a consequence of the elevated $[Ca^{2+}]_i$ and pH_i (Wang et al., 2012).

(E) and **(F)** Voltage clamp measurements from intact guard cells of the Arabidopsis *slac1* mutant before, during challenge with 300 mOsM mannitol, and 5 min after mannitol washout. Measurements performed in 10 mM KCl with 5 mM Ca-MES, pH 6.1. Voltage stepped from a holding potential of −100 mV in eight steps from −100 mV to +50 mV **(C)** for $I_{K,out}$ and to −250 mV **(D)** for $I_{K,in}$. Data are means ± SE of seven independent experiments. Curves are nonlinear least-squares fittings performed jointly for each current to Equation 2. Fittings yielded common voltage sensitivity coefficients (δ) of 1.79 ± 0.04 and 1.86 ± 0.09 for $I_{K,in}$ and $I_{K,out}$, respectively, and a common midpoint voltage ($V_{1/2}$) for $I_{K,out}$ of −2 ± 3 mV (see also Supplemental Table 2). Insets: Current traces from one guard cell, cross-referenced by symbol. Scale: 400 pA ($I_{K,out}$) and 100 pA ($I_{K,in}$) vertical, 1 s horizontal. Note the expanded current scale in **(F)** showing the suppressed $I_{K,in}$ in mannitol and the absence of a significant overshoot on its washout, as predicted. Currents from *pSLAC1* Arabidopsis were indistinguishable from the wild type (Figure 4) and are omitted for clarity.

and water transport. Recent studies support the idea that water in the guard cell wall is normally maintained by, and equilibrates with, the vapor phase within the intercellular air space of the leaf (Shope et al., 2008; Mott and Peak, 2010; Pieruschka et al., 2010; Rockwell et al., 2014). Since gaseous exchange within the leaf is extremely rapid (Sack and Holbrook, 2006; Morison et al., 2007; Peak and Mott, 2011), this equilibrium implies that the water potential of the guard cell wall is coupled directly to the surrounding air space within the substomatal cavity and it suggests a formal basis for connecting the macroscopic conductance of the leaf with the microscopic processes of the guard cell. We have integrated these ideas within OnGuard2 by ascribing the effects of increasing VPD to a local depression in water potential adjacent to the guard cells and by modeling evaporative demand as a simple linear function of water feed to the leaf and substomatal cavity. An analogous approach can be applied to resolving stomatal control by CO_2, which will be the focus of a subsequent publication. For now, we note the strength of this approach, which unifies stomatal mechanics within a single, computational framework that scales naturally from solute and water transport of the guard cell to the water relations of the leaf and whole plant.

OnGuard2 incorporates the core of our original OnGuard platform, which successfully recapitulated a wide range of known stomatal behaviors (Chen et al., 2012; Blatt et al., 2014; Minguet-Parramona et al., 2016) and demonstrated true predictive power, notably in resolving the mechanisms behind the counterintuitive alterations in K^+ channel activity uncovered in the *slac1* Cl^- channel mutant of Arabidopsis (Wang et al., 2012). Like the original platform, OnGuard2 utilizes an iterative computational approach and does not "hardwire" signal cascades beyond the immediate regulation of individual transporters and metabolic activities that have been well-defined through quantitative experimentation. While fixed or analytic solutions, including those for hormonal signaling, may appear to provide simplified or explicit equations for a process, they generally sterilize the predictive power of model implementation. Instead, OnGuard2 allows flexibility in model design to guide experimentation, reformulate, and validate predictions across scales.

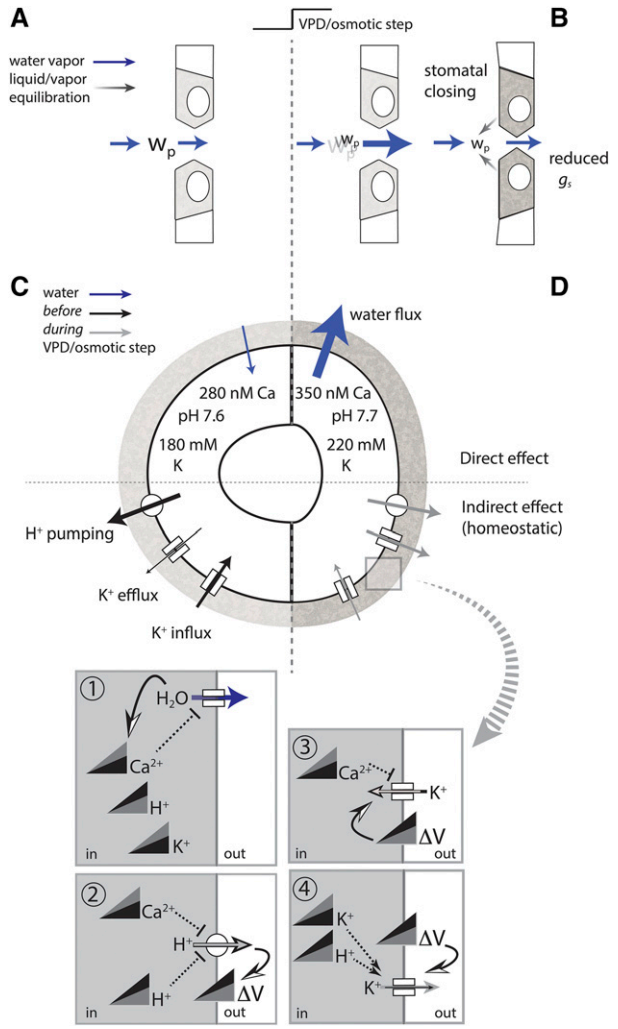

Figure 8. A Step Decrease in Partial Vapor Pressure of Water at *p*, w_p, or a Step Increase in the Osmotic Solute Load of the Apoplast Drives Stomatal Closure via Water Flux from the Guard Cell and Homeostatic Adjustment in Guard Cell Transport.

(A) and **(B)** At the macroscopic scale, steady state transpiration is balanced by evaporation (not shown) from within the leaf to maintain a constant w_p. A VPD step increases the rate of transpiration through the stomatal pore, decreasing w_p. Water in the apoplast around the guard cells reequilibrates with the reduced w_p within the substomatal cavity. The decline in water potential of the apoplast draws water out of the guard cell, leading to a decrease in guard cell volume and turgor and reduces the size of the stomatal pore (see Figure 2). Omitted for clarity, feedback via the reduced conductance of the stomatal pore counters and moderates the decline in w_p and water loss from the guard cell and surrounding apoplast. Darker shading in the apoplast around the guard cells indicates a decrease in water potential.

(C) and **(D)** At the microscopic scale, water influx accompanies solute accumulation, driven by the H^+-ATPase, to facilitate the increase in guard cell volume, turgor, and stomatal opening. As water is drawn out of the guard cell (1), either by a step increase in VPD or in apoplastic osmotic load, it reduces the cell volume and alters the concentrations of cellular solutes, including that of K^+, the free concentrations of cytosolic Ca^{2+} ($[Ca^{2+}]_i$) and $[H^+]_i$, raising pH_i. The rise in $[Ca^{2+}]_i$, especially, slows water flux. (2) The rise in $[Ca^{2+}]_i$ and pH_i reduces H^+-ATPase activity favoring membrane depolarization and initiating voltage oscillations (Minguet-Parramona et al., 2016) that readjust the contents of inorganic and organic solutes (see Figures 2 to 4 and Supplemental Figure 2). Contributing to this readjustment, the rise in $[Ca^{2+}]_i$ suppresses the activity of inward-rectifying K^+ channels (3), the rise in pH_i and cytosolic K^+ concentration promotes the activity of outward-rectifying K^+ channels (4), and voltage oscillations moderate K^+ (and other) solute flux with the transition to a new homeostatic steady state. Arrow weighting above indicates currents before (black arrows) and during (gray arrows) VPD/osmotic challenge. Water flux is indicated by blue arrows. Changes in ion concentrations in boxes below indicated by shading (black, before; gray, during VPD/osmotic challenge); process activation and inhibition are indicated by dotted arrows and T-bars, respectively.

OnGuard2 faithfully reproduced the experimentally determined kinetics and dependence of stomatal aperture and g_s on VPD and water availability, notably a weak dependence on VPD unless water delivery to the leaf was limited; it replicated the curvilinear effects of leaf temperature on aperture and g_s (Supplemental Figure 1) previously reported across a range of species in the literature (Wilson, 1948; Stalfelt, 1962; Farquhar and Sharkey, 1982; Spence et al., 1984; Urban et al., 2017); it showed the opposing changes in guard cell osmolarity and turgor (Figure 2) expected of a unified framework equating VPD to extracellular osmotic potential; and it recapitulated previously published data of enhanced Mal synthesis and accumulation with osmotic stress (Asai et al., 1999, 2000). Noteworthy to these predictions, within OnGuard2 it is the change in water potential of the apoplast around the guard cell with a VPD step that drives water flux across the guard cell plasma membrane, thereby affecting guard cell volume, the free concentration of solute within the guard cell, and engaging changes in ion transport and metabolism (Figure 8). In other words, for VPD, it is the change in the partial vapor pressure of water that drives guard cell function.

However, the true power of the OnGuard2 models is evident in the experimental validations of their predictions connecting g_s and stomatal aperture with solute transport. This predictive power is evident both in the effects of VPD steps on guard cell transport and, vice versa, in the consequences of altered ion transport on VPD-evoked stomatal movements and g_s. Compared with the wild type, OnGuard2 models of the *slac1* Cl^- channel and *ost2* H^+-ATPase mutants accurately predicted substantial slowing in the rates of stomatal closure and of g_s decline and, for the *ost2* mutant, in g_s recovery. In *slac1*, OnGuard2 also correctly predicted an accelerated recovery in aperture and g_s, an unexpected prediction that contrasts with the slowed opening modeled and observed experimentally in response to light (Wang et al., 2012). The same models predicted an enhancement of $I_{K,out}$ and decline in $I_{K,in}$ with an increase in VPD and external osmolarity, and counterintuitive overshoots in $I_{K,in}$ on their recovery that were verified under voltage clamp (Figures 4 to 7). For the *ost2* mutant, like *slac1* (Wang et al., 2012), these effects are linked to $[Ca^{2+}]_i$ and pH_i, predictions that were borne out experimentally (Figures 6 and 9). The effects on the K^+ currents, like the impact of the *slac1* and *ost2* mutants on g_s, clearly arise as emergent properties of guard cell transport and its connection with VPD-evoked water flux and volume changes and

are beyond intuitive grasp. Only a mechanistic model spanning the micro-macro scales can predict and explain these results, accommodating the very different natures of the two mutants (Merlot et al., 2007; Wang et al., 2012; Blatt et al., 2014).

VPD-driven changes in guard cell volume connect with ion transport through the concurrent effects on ion concentration within the cytosol and vacuole, notably through changes in $[Ca^{2+}]_i$ and pH_i, both of which are known to affect the osmotic conductance of the plasma membrane (Alleva et al., 2006; Verdoucq et al., 2008; Bellati et al., 2010; Maurel et al., 2015). In OnGuard2, such regulatory feedback is incorporated explicitly. OnGuard2 models explain the rise in $[Ca^{2+}]_i$ and consequent decline in the Ca^{2+}-sensitive $I_{K,in}$ (Grabov and Blatt, 1999; Jezek and Blatt, 2017) as the direct consequence of increasing external osmolarity, which reduces guard cell volume and raises the total concentration of Ca^{2+} and all other cellular solutes. Likewise, the models ascribe the pH_i rise to the elevated Mal concentration that contributes to H^+ buffering (Wang et al., 2012; Jezek and Blatt, 2017). Together with the osmotically induced rise in $[K^+]_i$, the pH_i rise promotes $I_{K,out}$ (Grabov and Blatt, 1997; Hosy et al., 2003). These models also explain the suppressed $[Ca^{2+}]_i$ and overshoot in $I_{K,in}$ when VPD and osmotic challenges are reversed; the effects follow from transport that rebalances $[Ca^{2+}]_i$, notably an initial, compensatory bias for Ca^{2+} export across the tonoplast and plasma membrane with elevated VPD and external osmotic strength.

For the *slac1* and *ost2* mutants, OnGuard2 predicted alterations in transport, raising $[Ca^{2+}]_i$ and pH_i well above the K_{Ca} of $I_{K,in}$ and below the K_H of $I_{K,out}$, effects that, again, we verified experimentally (Figures 5, 6, and 9; also Wang et al. [2012] for *slac1*). Such elevations largely preempt the effects on the K^+ currents of further changes in $[Ca^{2+}]_i$ and pH_i with VPD and osmotic challenge. In these models, the rise in background $[Ca^{2+}]_i$ was also predicted to reduce the rates of osmotic water flux, further affecting the kinetics of VPD-evoked aperture and g_s changes. These are only a small sample of the predictions that come out of the OnGuard2 models. Others include effects of VPD and external osmolarity on the plasma membrane anion channels, on vacuolar $[Ca^{2+}]$, and on Ca^{2+} and osmotic solute transport across the tonoplast. Such predictions are now targets for future exploration that should also help to refine OnGuard2 models.

We stress that our findings do not rule out additional mechanisms, such as might occur through more subtle changes in phosphorylation (Grondin et al., 2015) or ABA synthesis (McAdam and Brodribb, 2016). The results indicate only that any such changes are not, in themselves, essential to understanding stomatal movements with VPD and external osmotic strength. Bauer et al. (2013) have argued that ABA is essential for stomatal response to VPD. However, they never measured stomatal aperture or g_s. Their comparison of gene expression between the wild type and mutant that impairs ABA synthesis is based on samples taken 4 h after a VPD step, although stomatal response to the same VPD step was largely complete within 60 min, and their own data for potassium content, which they proposed as a proxy for stomatal aperture, indicating that the mutant plants were as, or more, sensitive to VPD than the wild-type plants when compared with the corresponding contents determined at high humidity. We note that their analysis of the K^+ contents in frozen tissues is at odds with our assays of guard cell K^+ concentrations under osmotic challenge in vivo. Furthermore, the interpretation of a requirement for ABA is not supported by several other studies, indicating that stomata do respond quasi-normally to VPD in the absence of ABA biosynthesis and ABA signaling through the ABI1/ABI2 protein phosphatase pathways (Assmann et al., 2000; Pantin et al., 2013).

Like our previous work with OnGuard (Wang et al., 2012), the predictions derived from OnGuard2 and their experimental validations underscore an intimate connection of the K^+ channels with the mechanistically separate activities of the SLAC1 Cl^- channel and AHA1 H^+-ATPase. Most important, however, our study demonstrates the capacity of a single, computational framework to connect the microscopic processes of membrane transport in the guard cell with the macroscopic water relations of the leaf and whole plant. This development paves the way to

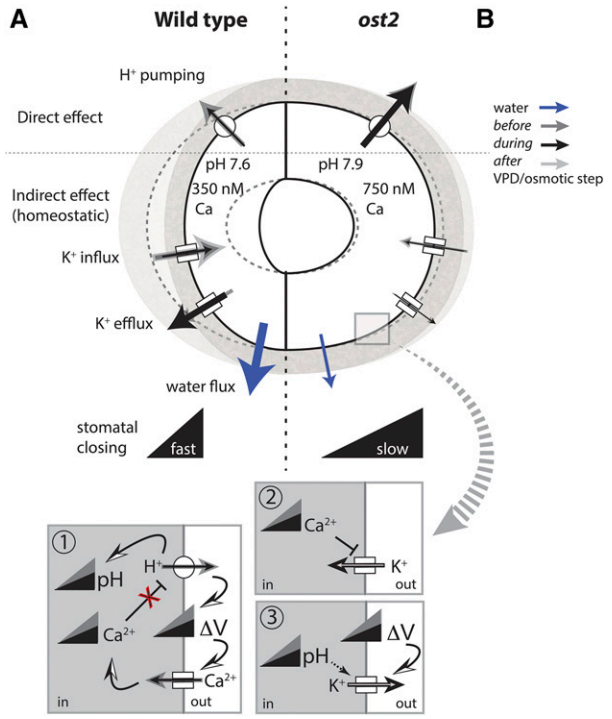

Figure 9. The *ost2* Mutant H^+-ATPase Affects K^+ Channel Activities and the Rates of Stomatal and Whole-Leaf Conductance Responses to Steps in VPD between the Air Space within the Leaf and the Atmosphere.

Tonoplast and other transporters are not included for clarity.
(A) The H^+-ATPase is a major driver for solute uptake, and its modulation by elevated free cytosolic $[Ca^{2+}]$ ($[Ca^{2+}]_i$) is important to accelerate stomatal closure. The K^+ channel currents $I_{K,in}$ (K^+ influx) and $I_{K,out}$ (K^+ efflux) facilitate osmotic solute uptake during opening and its loss during closing, respectively. Arrow shading above indicates temporal characteristics before (dark gray), during (black), and after (light gray) VPD and osmotic steps.
(B) The *ost2* mutation renders the H^+-ATPase insensitive to a rise in $[Ca^{2+}]_i$ and suppresses membrane depolarization, promoting a rise in cytosolic pH (pH_i) as well as Ca^{2+} entry, background $[Ca^{2+}]_i$ elevation, and its rise with VPD (1). Elevated $[Ca^{2+}]_i$ in turn suppresses background $I_{K,in}$ and reduces its response to VPD (2). The rise in cytosolic pH (pH_i) promotes background $I_{K,out}$ and reduces its response with VPD. With the Ca^{2+}-insensitive H^+-ATPase, channel activation and K^+ efflux are suppressed by membrane voltage (3) along with water efflux, thereby slowing stomatal and g_s kinetics.

addressing many other aspects of stomatal physiology, and it is certain to yield a greater understanding of fundamental and mutual connections between plant water relations and guard cell membrane transport.

METHODS

Growth and Whole-Plant Physiology

Arabidopsis thaliana Col-0 wild type, *slac1-1*, *ProSLAC1:SLAC1*-complemented *slac1-1* mutant, designated *pSLAC1*, and *ost2-2* mutant plants were grown and gas exchange measurements were performed using LiCOR 6400XT and 6800 gas exchange systems as described previously (Merlot et al., 2007; Wang et al., 2012) with plants preadapted to dark. Relative water content of the soil was determined using a HH2-ML3 moisture sensor (Delta-T Devices). All plants were analyzed on at least three separate days at the same time of the relative diurnal cycle and were normalized for leaf area using ImageJ v.1.51 (rsbweb.nih.gov/ij/). Unless otherwise noted, all measurements were performed at 25°C.

Gene Expression Analysis

Total RNA was extracted from mature leaves and transcript levels determined by quantitative PCR as before (Wang et al., 2012) using unique primers (Supplemental Table 1) for the plasma membrane channels *KAT1*, *KAT2*, *KC1*, *GORK*, *AKT1*, *AKT2*, and *SLAC1*, and the vacuolar channels *TPK1* and *TPC1*. The *ISU* gene encoding an Fe-S scaffolding protein (Kaiserli et al., 2015) served as an internal control.

Guard Cell Electrophysiology, $[Ca^{2+}]_i$, and pH_i Recording

Currents from intact guard cells were recorded under voltage clamp using double- and triple-barrelled microelectrodes and Henry's EP suite (Y-Science) during continuous superfusion with 10 mM KCl in 5 mM Ca^{2+}-MES buffer, pH 6.1 ($[Ca^{2+}]$ = 1 mM) as before (Wang et al., 2012). Voltage was typically clamped in cycles with a holding voltage of −100 mV and steps either to voltages from −120 to −240 mV ($I_{K,in}$) or to voltages from −80 to +40 mV ($I_{K,out}$). Current-voltage analysis and fittings were performed using Henry's EP suite (Y-Science) and SigmaPlot 11 (Systat Software). Currents were fitted by joint, nonlinear least-squares using the Boltzmann function of Equation 2. Cytosolic-free $[Ca^{2+}]$ and pH_i were determined by fluorescence ratio imaging after iontophoretic injection of the fluorescent dyes Fura2 and BCECF, respectively, using a Polychrom II monochromator (Till Photonics) and Pentamax512 CCD camera and GenIV intensifier (Princeton Instruments) as described previously (Wang et al., 2012). Fluorescence was corrected for background before loading, dye injections were judged successful by visual checks for cytosolic dye distribution and stabilization of the fluorescence signals, and signals were calibrated as before (Grabov and Blatt, 1999; Wang et al., 2012).

OnGuard2 Modeling

OnGuard2 was constructed to introduce explicitly water feed to, and evapotranspiration from, the leaf, leaf and air temperatures, as well as water flux across the guard cell plasma membrane as described in the Appendix. The construction used the core of the original OnGuard libraries for solute transport, signaling, and homeostasis (Chen et al., 2012; Hills et al., 2012; Wang et al., 2012) with separate assignments of blue and red light (Vialet-Chabrand et al., 2017).

OnGuard2 models for wild-type Arabidopsis and the *slac1* and *ost2* mutants were driven through a diurnal 12:12-h light:dark cycle as described previously (Chen et al., 2012; Wang et al., 2012; Blatt et al., 2014), and all model outputs were derived from this cycle. Leaf and air temperatures, T_{leaf} and T_{air}, respectively, were held at 25°C unless otherwise noted. RWF and mid-day steps in w_{air} were superimposed on this cycle. As in the original formulation of OnGuard, light sensitivity was assigned solely to primary, energy-dependent transport and to sucrose synthesis (Chen et al., 2012; Hills et al., 2012; Wang et al., 2012). To simulate the two mutants, in the corresponding models we removed the transporter component of the SLAC1 current for *slac1*, and we removed the $[Ca^{2+}]_i$ sensitivity of the plasma membrane H^+-ATPase for *ost2* (Wang et al., 2012; Blatt et al., 2014). All other parameters were fixed as in the wild-type model. The outputs of the individual transporters, sucrose and malate metabolism, buffering reactions, and transpirational water flux thus responded only to changes in model variables arising from the kinetic features encoded by the model equations and their parameters. A complete list of parameter values used for the Arabidopsis wild-type model is included in Supplemental Appendix 1. OnGuard2 and the models for Arabidopsis wild type, *slac1*, and *ost2* are available for free download from www.psrg.org.uk.

Statistics

Results are reported as means ± SE of *n* observations with significance determined by ANOVA, as appropriate, with post-hoc analysis (Student-Neumann-Keuls and Tukey), and are indicated at $P < 0.05$ unless otherwise stated. Note that models built on ordinary differential equations, such as those of OnGuard2, will faithfully reproduce a given set of outputs time and again for any one set of model parameters. Statistical analysis of these outputs is therefore meaningless.

Accession Numbers

Sequence data from this article can be obtained from the Arabidopsis Genome Initiative databases under the following accession numbers: *KAT1*, AT5G46240; *KAT2*, AT4G18290; *KC1*, AT4G32650; *GORK*, AT5G37500; *AKT1*, AT2G26650; *AKT2*, AT4G22200; *SLAC1*, AT1G12480; *TPK1*, AT5G55630; and *TPC1*, AT4G03560.

Supplemental Data

Supplemental Figure 1. OnGuard2 yields a curvilinear dependence of stomatal conductance (g_s) on temperature and the partial vapor pressure of water in the air (w_{air}).

Supplemental Figure 2. OnGuard2 outputs for guard cell pH, Ca^{2+}, osmotic solute transport, and Mal synthesis of the wild type.

Supplemental Figure 3. OnGuard2 outputs for guard cell pH, Ca^{2+}, osmotic solute transport, and Mal synthesis of the *ost2* mutant.

Supplemental Figure 4. Quantitative PCR analysis of selected plasma membrane and tonoplast transporter genes in the *ost2* mutant of Arabidopsis.

Supplemental Table 1. qPCR primers

Supplemental Table 2. Parameters derived from Boltzmann fittings for K^+ currents from guard cells of wild-type plants and the mutants *ost2* and *slac1.*

Supplemental Appendix 1. OnGuard2 Arabidopsis model parameters.

ACKNOWLEDGMENTS

This work was supported by Biotechnology and Biological Sciences Research Council (BBSRC) Grants BB/L019205/1 and BB/M001601/1 to M.R.B., BB/L001276/1 to M.R.B. and S.R., and BB/I001187/1 to H.G. and T.L.

AUTHOR CONTRIBUTIONS

Y.W., S.V.-C., M.R.B., and M.P. carried out voltage clamp, gas exchange, $[Ca^{2+}]_i$, and pH_i measurements and qPCR experiments, and analyzed the results. V.L.L., A.H., and M.R.B. developed the OnGuard2 structure. M.P., H.G., S.R., and T.L. contributed to writing the manuscript with V.L.L., A.H., and M.R.B.

Received September 5, 2017; revised October 11, 2017; accepted October 31, 2017; published November 1, 2017.

REFERENCES

Alleva, K., Niemietz, C.M., Sutka, M., Maurel, C., Parisi, M., Tyerman, S.D., and Amodeo, G. (2006). Plasma membrane of *Beta vulgaris* storage root shows high water channel activity regulated by cytoplasmic pH and a dual range of calcium concentrations. J. Exp. Bot. **57:** 609–621.

Asai, N., Nakajima, N., Kondo, N., and Kamada, H. (1999). The effect of osmotic stress on the solutes in guard cells of *Vicia faba* L. Plant Cell Physiol. **40:** 843–849.

Asai, N., Nakajima, N., Tamaoki, M., Kamada, H., and Kondo, N. (2000). Role of malate synthesis mediated by phosphoenolpyruvate carboxylase in guard cells in the regulation of stomatal movement. Plant Cell Physiol. **41:** 10–15.

Assmann, S.M., and Jegla, T. (2016). Guard cell sensory systems: recent insights on stomatal responses to light, abscisic acid, and CO_2. Curr. Opin. Plant Biol. **33:** 157–167.

Assmann, S.M., Snyder, J.A., and Lee, Y.R.J. (2000). ABA-deficient (aba1) and ABA-insensitive (abi1-1, abi2-1) mutants of Arabidopsis have a wild-type stomatal response to humidity. Plant Cell Environ. **23:** 387–395.

Bauer, H., et al. (2013). The stomatal response to reduced relative humidity requires guard cell-autonomous ABA synthesis. Curr. Biol. **23:** 53–57.

Bellati, J., Alleva, K., Soto, G., Vitali, V., Jozefkowicz, C., and Amodeo, G. (2010). Intracellular pH sensing is altered by plasma membrane PIP aquaporin co-expression. Plant Mol. Biol. **74:** 105–118.

Blatt, M.R. (2000). Cellular signaling and volume control in stomatal movements in plants. Annu. Rev. Cell Dev. Biol. **16:** 221–241.

Blatt, M.R., and Clint, G.M. (1989). Fusicoccin activates energy-coupled K^+ uptake by stomatal guard cells. Plant Physiol. **89:** 1169A.

Blatt, M.R., Thiel, G., and Trentham, D.R. (1990). Reversible inactivation of K^+ channels of Vicia stomatal guard cells following the photolysis of caged inositol 1,4,5-trisphosphate. Nature **346:** 766–769.

Blatt, M.R., Wang, Y., Leonhardt, N., and Hills, A. (2014). Exploring emergent properties in cellular homeostasis using OnGuard to model K^+ and other ion transport in guard cells. J. Plant Physiol. **171:** 770–778.

Bowling, D.J.F. (1987). Measurement of the apoplastic activity of K+ and Cl− in the leaf epidermis of *Commelina communis* in relation to stomatal activity. J. Exp. Bot. **38:** 1351–1355.

Buckley, T.N. (2005). The control of stomata by water balance. New Phytol. **168:** 275–292.

Buckley, T.N., and Mott, K.A. (2002). Dynamics of stomatal water relations during the humidity response: implications of two hypothetical mechanisms. Plant Cell Environ. **25:** 407–419.

Buckley, T.N., Mott, K.A., and Farquhar, G.D. (2003). A hydromechanical and biochemical model of stomatal conductance. Plant Cell Environ. **26:** 1767–1785.

Buckley, T.N., John, G.P., Scoffoni, C., and Sack, L. (2017). The sites of evaporation within leaves. Plant Physiol. **173:** 1763–1782.

Bush, D.S., and McColl, J.G. (1987). Mass-action expressions of ion exchange applied to Ca^{2+}, H^+, K^+ and Mg^{2+} sorption on isolated cell walls of leaves from *Brassica oleracea*. Plant Physiol. **85:** 247–260.

Caldeira, C.F., Jeanguenin, L., Chaumont, F., and Tardieu, F. (2014). Circadian rhythms of hydraulic conductance and growth are enhanced by drought and improve plant performance. Nat. Commun. **5:** 5365.

Chaumont, F., and Tyerman, S.D. (2014). Aquaporins: highly regulated channels controlling plant water relations. Plant Physiol. **164:** 1600–1618.

Chen, Z.H., Hills, A., Bätz, U., Amtmann, A., Lew, V.L., and Blatt, M.R. (2012). Systems dynamic modeling of the stomatal guard cell predicts emergent behaviors in transport, signaling, and volume control. Plant Physiol. **159:** 1235–1251.

Dewar, R.C. (1995). Interpretation of an empirical model for stomatal conductance in terms of guard-cell function. Plant Cell Environ. **18:** 365–372.

Farquhar, G.D. (1978). Feedforward responses of stomata to humidity. Aust. J. Plant Physiol. **5:** 787–800.

Farquhar, G.D., and Sharkey, T.D. (1982). Stomatal conductance and photosynthesis. Annu. Rev. Plant Physiol. Plant Mol. Biol. **33:** 317–345.

Farquhar, G.D., von Caemmerer, S., and Berry, J.A. (2001). Models of photosynthesis. Plant Physiol. **125:** 42–45.

Findlay, G.P., and Hope, A.B. (1976). Electrical properties of plant cells: methods and findings. In Encyclopedia of Plant Physiology, Vol. 2A, U. Luettge and M.G. Pitman, eds (Berlin: Springer Verlag), pp. 53–92.

Grabov, A., and Blatt, M.R. (1997). Parallel control of the inward-rectifier K^+ channel by cytosolic-free Ca^{2+} and pH in Vicia guard cells. Planta **201:** 84–95.

Grabov, A., and Blatt, M.R. (1998). Membrane voltage initiates Ca^{2+} waves and potentiates Ca^{2+} increases with abscisic acid in stomatal guard cells. Proc. Natl. Acad. Sci. USA **95:** 4778–4783.

Grabov, A., and Blatt, M.R. (1999). A steep dependence of inward-rectifying potassium channels on cytosolic free calcium concentration increase evoked by hyperpolarization in guard cells. Plant Physiol. **119:** 277–288.

Grignon, C., and Sentenac, H. (1991). pH and ionic conditions in the apoplast. Annu. Rev. Plant Physiol. Plant Mol. Biol. **42:** 103–128.

Grondin, A., Rodrigues, O., Verdoucq, L., Merlot, S., Leonhardt, N., and Maurel, C. (2015). Aquaporins contribute to ABA-triggered stomatal closure through OST1-mediated phosphorylation. Plant Cell **27:** 1945–1954.

Hill, B.S., and Findlay, G.P. (1981). The power of movement in plants: the role of osmotic machines. Q. Rev. Biophys. **14:** 173–222.

Hills, A., Chen, Z.H., Amtmann, A., Blatt, M.R., and Lew, V.L. (2012). OnGuard, a computational platform for quantitative kinetic modeling of guard cell physiology. Plant Physiol. **159:** 1026–1042.

Holdaway-Clarke, T.L., and Hepler, P.K. (2003). Control of pollen tube growth: role of ion gradients and fluxes. New Phytol. **159:** 539–563.

Hosy, E., et al. (2003). The Arabidopsis outward K^+ channel GORK is involved in regulation of stomatal movements and plant transpiration. Proc. Natl. Acad. Sci. USA **100:** 5549–5554.

Jezek, M., and Blatt, M.R. (2017). The membrane transport system of the guard cell and its integration for stomatal dynamics. Plant Physiol. **174:** 487–519.

Kaiserli, E., Páldi, K., O'Donnell, L., Batalov, O., Pedmale, U.V., Nusinow, D.A., Kay, S.A., and Chory, J. (2015). Integration of light and photoperiodic signaling in transcriptional nuclear foci. Dev. Cell **35:** 311–321.

Kim, T.H., Böhmer, M., Hu, H., Nishimura, N., and Schroeder, J.I. (2010). Guard cell signal transduction network: advances in understanding abscisic acid, CO_2, and Ca^{2+} signaling. Annu. Rev. Plant Biol. **61:** 561–591.

Lange, O.L., Lösch, R., Schulze, E.D., and Kappen, L. (1971). Responses of stomata to changes in humidity. Planta **100:** 76–86.

Lawson, T., and Blatt, M.R. (2014). Stomatal size, speed, and responsiveness impact on photosynthesis and water use efficiency. Plant Physiol. **164:** 1556–1570.

Lemtiri-Chlieh, F., and MacRobbie, E.A.C. (1994). Role of calcium in the modulation of Vicia guard cell potassium channels by abscisic acid: a patch-clamp study. J. Membr. Biol. **137:** 99–107.

Lew, V.L., and Bookchin, R.M. (1986). Volume, pH, and ion-content regulation in human red cells: analysis of transient behavior with an integrated model. J. Membr. Biol. **92:** 57–74.

Lew, V.L., Ferreira, H.G., and Moura, T. (1979). The behaviour of transporting epithelial cells. I. Computer analysis of a basic model. Proc. R. Soc. Lond. B Biol. Sci. **206:** 53–83.

Locke, A.M., and Ort, D.R. (2015). Diurnal depression in leaf hydraulic conductance at ambient and elevated CO_2 reveals anisohydric water management in field-grown soybean and possible involvement of aquaporins. Environ. Exp. Bot. **116:** 39–46.

Maier-Maercker, U. (1983). The role of peristomatal transpiration in the mechanism of stomatal movement. Plant Cell Environ. **6:** 369–380.

Marschner, H. (1995). Mineral Nutrition of Higher Plants. (New York: Academic Press).

Marten, H., Konrad, K.R., Dietrich, P., Roelfsema, M.R.G., and Hedrich, R. (2007). Ca^{2+}-dependent and -independent abscisic acid activation of plasma membrane anion channels in guard cells of *Nicotiana tabacum*. Plant Physiol. **143:** 28–37.

Maurel, C. (1997). Aquaporins and water permeability of plant membranes. Annu. Rev. Plant Physiol. Plant Mol. Biol. **48:** 399–429.

Maurel, C., Boursiac, Y., Luu, D.T., Santoni, V., Shahzad, Z., and Verdoucq, L. (2015). Aquaporins in plants. Physiol. Rev. **95:** 1321–1358.

Mauritz, J.M.A., Esposito, A., Ginsburg, H., Kaminski, C.F., Tiffert, T., and Lew, V.L. (2009). The homeostasis of *Plasmodium falciparum*-infected red blood cells. PLOS Comput. Biol. **5:** e1000339.

McAdam, S.A.M., and Brodribb, T.J. (2016). Linking turgor with ABA biosynthesis: implications for stomatal responses to vapor pressure deficit across land plants. Plant Physiol. **171:** 2008–2016.

McAinsh, M.R., and Pittman, J.K. (2009). Shaping the calcium signature. New Phytol. **181:** 275–294.

Merilo, E., Laanemets, K., Hu, H., Xue, S., Jakobson, L., Tulva, I., Gonzalez-Guzman, M., Rodriguez, P.L., Schroeder, J.I., Broschè, M., and Kollist, H. (2013). PYR/RCAR receptors contribute to ozone-, reduced air humidity-, darkness-, and CO_2-induced stomatal regulation. Plant Physiol. **162:** 1652–1668.

Merlot, S., Leonhardt, N., Fenzi, F., Valon, C., Costa, M., Piette, L., Vavasseur, A., Genty, B., Boivin, K., Müller, A., Giraudat, J., and Leung, J. (2007). Constitutive activation of a plasma membrane H^+-ATPase prevents abscisic acid-mediated stomatal closure. EMBO J. **26:** 3216–3226.

Minguet-Parramona, C., Wang, Y., Hills, A., Vialet-Chabrand, S., Griffiths, H., Rogers, S., Lawson, T., Lew, V.L., and Blatt, M.R. (2016). An optimal frequency in Ca^{2+} oscillations for stomatal closure is an emergent property of ion transport in guard cells. Plant Physiol. **170:** 33–42.

Morison, J.I.L., Lawson, T., and Cornic, G. (2007). Lateral CO_2 diffusion inside dicotyledonous leaves can be substantial: quantification in different light intensities. Plant Physiol. **145:** 680–690.

Mott, K.A. (2007). Leaf hydraulic conductivity and stomatal responses to humidity in amphistomatous leaves. Plant Cell Environ. **30:** 1444–1449.

Mott, K.A., and Peak, D. (2010). Stomatal responses to humidity and temperature in darkness. Plant Cell Environ. **33:** 1084–1090.

Murai-Hatano, M., and Kuwagata, T. (2007). Osmotic water permeability of plasma and vacuolar membranes in protoplasts I: high osmotic water permeability in radish (*Raphanus sativus*) root cells as measured by a new method. J. Plant Res. **120:** 175–189.

Nobel, P.S. (2012). Physicochemical and Environmental Plant Physiology. (San Diego: Academic Press).

Pantin, F., Monnet, F., Jannaud, D., Costa, J.M., Renaud, J., Muller, B., Simonneau, T., and Genty, B. (2013). The dual effect of abscisic acid on stomata. New Phytol. **197:** 65–72.

Peak, D., and Mott, K.A. (2011). A new, vapour-phase mechanism for stomatal responses to humidity and temperature. Plant Cell Environ. **34:** 162–178.

Pieruschka, R., Huber, G., and Berry, J.A. (2010). Control of transpiration by radiation. Proc. Natl. Acad. Sci. USA **107:** 13372–13377.

Prado, K., Boursiac, Y., Tournaire-Roux, C., Monneuse, J.-M., Postaire, O., Da Ines, O., Schäffner, A.R., Hem, S., Santoni, V., and Maurel, C. (2013). Regulation of Arabidopsis leaf hydraulics involves light-dependent phosphorylation of aquaporins in veins. Plant Cell **25:** 1029–1039.

Rockwell, F.E., Holbrook, N.M., and Stroock, A.D. (2014). The competition between liquid and vapor transport in transpiring leaves. Plant Physiol. **164:** 1741–1758.

Roelfsema, M.R., and Hedrich, R. (2010). Making sense out of Ca^{2+} signals: their role in regulating stomatal movements. Plant Cell Environ. **33:** 305–321.

Sack, L., and Holbrook, N.M. (2006). Leaf hydraulics. Ann. Rev. Plant Biol **57:** 361–381.

Sanders, D., Pelloux, J., Brownlee, C., and Harper, J.F. (2002). Calcium at the crossroads of signaling. Plant Cell **14** (suppl.): S401–S417.

Segel, I.H. (1993). Enzyme Kinetics. (New York: Wiley Interscience).

Shope, J.C., Peak, D., and Mott, K.A. (2008). Stomatal responses to humidity in isolated epidermes. Plant Cell Environ. **31:** 1290–1298.

Smith, N.G., and Dukes, J.S. (2013). Plant respiration and photosynthesis in global-scale models: incorporating acclimation to temperature and CO_2. Glob. Change Biol. **19:** 45–63.

Spence, R.D., Sharpe, P.J.H., Powell, R.D., and Wu, H. (1984). Response of guard cells to temperature at different concentrations of carbon dioxide in *Vica faba* L. New Phytol. **97:** 129–144.

Stalfelt, M.G. (1962). The effect of temperature on opening of the stomatal cells. Physiol. Plant. **15:** 772–779.

Taiz, L. (1984). Plant-cell expansion - regulation of cell-wall mechanical-properties. Annu. Rev. Plant Physiol. Plant Mol. Biol. **35:** 585–657.

Tournaire-Roux, C., Sutka, M., Javot, H., Gout, E., Gerbeau, P., Luu, D.T., Bligny, R., and Maurel, C. (2003). Cytosolic pH regulates root water transport during anoxic stress through gating of aquaporins. Nature **425:** 393–397.

Urban, J., Ingwers, M.W., McGuire, M.A., and Teskey, R.O. (2017). Increase in leaf temperature opens stomata and decouples net photosynthesis from stomatal conductance in *Pinus taeda* and *Populus deltoides* x *nigra*. J. Exp. Bot. **68:** 1757–1767.

Verdoucq, L., Grondin, A., and Maurel, C. (2008). Structure-function analysis of plant aquaporin AtPIP2;1 gating by divalent cations and protons. Biochem. J. **415:** 409–416.

Vialet-Chabrand, S., Hills, A., Wang, Y., Griffiths, H., Lew, V.L., Lawson, T., Blatt, M.R., and Rogers, S. (2017). Global sensitivity analysis of OnGuard models identifies key hubs for transport interaction in stomatal dynamics. Plant Physiol. **174:** 680–688.

Wang, Y., Papanatsiou, M., Eisenach, C., Karnik, R., Williams, M., Hills, A., Lew, V.L., and Blatt, M.R. (2012). Systems dynamic modeling of a guard cell Cl^- channel mutant uncovers an emergent homeostatic network regulating stomatal transpiration. Plant Physiol. **160:** 1956–1967.

Willmer, C., and Fricker, M.D. (1996). Stomata. (London: Chapman and Hall), pp. 1–375.

Wilson, C.C. (1948). The effect of some environmental factors on the movements of guard cells. Plant Physiol. **23:** 5–37.

Yang, H.M., Zhang, X.Y., Tang, Q.L., and Wang, G.X. (2006a). Extracellular calcium is involved in stomatal movement through the regulation of water channels in broad bean. Plant Growth Regul. **50:** 79–83.

Yang, H.M., Zhang, X.Y., Wang, G.X., and Zhang, J.H. (2006b). Water channels are involved in stomatal oscillations encoded by parameter-specific cytosolic calcium oscillations. J. Integr. Plant Biol. **48:** 790–799.

Yuan, F., et al. (2014). OSCA1 mediates osmotic-stress-evoked Ca^{2+} increases vital for osmosensing in Arabidopsis. Nature **514:** 367–371.

APPENDIX

Deriving OnGuard2 with Micro-Macro Coupling

General Construction and Operation of the OnGuard2 Platform

OnGuard2 builds on the libraries of physical constants, metabolic, transport, and buffering equations, and user-defined parameters developed with the original OnGuard platform (Chen et al., 2012; Hills et al., 2012; Blatt et al., 2014). The equations and associated parameters are available through a graphic user interface (GUI) and series of pull-down menus that allow the user to define the basic flux and regulatory characteristics of each metabolic and transport process, and even to construct new transporters when information of physiological relevance becomes available through experimentation. The GUI provides users access to cellular parameters relating cell volume, turgor pressure, and stomatal aperture; it specifies the various transporters at each membrane and defines the characteristics for Suc and Mal metabolism; and it determines general environmental parameters of extracellular ion concentrations, the light: dark cycle and its spectral characteristics, and the time. Dialogue boxes for each transporter include operator-selectable controls for the inherent biophysical properties of the transporter as well as any known regulatory features. A complete description of this core of libraries and their implementation can be found in Hills et al. (2012).

New to OnGuard2 and incorporated within the core libraries is the class of transporters, aquaporins, that mediate the flux of water. The descriptors for aquaporins include options to define the fraction of the water flux carried by each type of aquaporin and to define its regulation by model variables such as $[Ca^{2+}]_i$. Also new to OnGuard2 are user-defined parameters needed to relate the guard cell to the leaf and whole plant and to determine the drivers for evapotranspiration. These include global parameters that specify the geometry of the stoma and its spatial relations to the underlying structure of the leaf—notably the fractional air space within the leaf and its dimensions—as well as water feed to the leaf and the partial pressure of water vapor in the air outside the leaf. We give the user access to leaf and external air temperatures, previously fixed to a standard 25°C (298°K) and used in all calculations involving temperature. For completeness, we also introduce temperature dependence for Suc and Mal metabolism with a user-defined parameter for Q_{10} (Segel, 1993).

OnGuard2 uses the same iterative computational strategy that was applied successfully in our original implementation of the OnGuard platform (Chen et al., 2012; Hills et al., 2012; Blatt et al., 2014) and, in the past, in other physiological systems (Lew et al., 1979; Lew and Bookchin, 1986; Mauritz et al., 2009). In operation, OnGuard2 calculates and logs the dynamic adjustments of ion flux, compartmental composition, and membrane voltage using the sets of constants, nonlinear differential equations, and parameters contained within the model, while obeying the fundamental physical constraints of mass and charge conservation. Running a simulation begins with a user-defined protocol representing the experiment or physiological effect under investigation from which the platform increments over small time intervals, typically 1 to 10 ms. With each time increment, OnGuard2 calculates the flux through each process and then uses the sums of each of the ionic and metabolic fluxes to determine the new values of membrane voltage and the contents of each compartment. It also calculates the diffusion of water vapor through the stomatal pore and the partial pressure of water vapor at p and, from these variables and the cell wall solute content, the water potential of the cell wall in equilibrium with the water vapor within the substomatal cavity. OnGuard2 uses these outputs and the total solute content of the guard cell at the end of each time interval to calculate the new total and compartmental cell volumes and ion concentrations, the guard cell turgor, and stomatal aperture.

Outputs of the ion concentrations of each compartment, plasma membrane, and tonoplast voltages, as well as stomatal aperture, g_s, and related variables are available in real time onscreen. The user is able to log these outputs, along with the flux through each transporter and metabolic reaction, in comma-delimited format that can be read by spreadsheet programs such as Microsoft Excel and SigmaPlot. Finally, the user has access to real-time displays of the current-voltage relations for each of the charge-carrying transporters at the plasma membrane and tonoplast, as well as the total membrane current, all of which are also available for download.

In implementing OnGuard2, we bridge the gap from the guard cell to whole-plant evapotranspiration with three critical developments encapsulated in mathematical formulations (1) that couple the guard cell to transpiration, (2) that account for water delivery to the leaf, and (3) that address water flux across the guard cell plasma membrane. The reasoning behind each development and the associated assumptions are set out in the main text. Here, we summarize the mathematical formulations that are incorporated within the new OnGuard2 libraries of constants, nonlinear differential equations, and parameters. A complete list of abbreviations for the various parameters and constants can be found in Appendix Table 1.

Connecting the Vapor Phase with Guard Cell Water

We define stomatal dynamics initially by the gain and loss of osmotically active solutes and water within the guard cell via transport across the plasma membrane and tonoplast, and by the synthesis and breakdown of Suc and Mal; solute content is then related through experimentally defined equations to guard cell volume, turgor, and stomatal aperture (Hills et al., 2012). The tonoplast cannot sustain hydrostatic pressure differences, and its permeability to water is high (Hill and Findlay, 1981; Willmer and Fricker, 1996; Maurel, 1997; Nobel, 2012; Chaumont and Tyerman, 2014; Maurel et al., 2015), so we assume that the osmotic pressure difference between the vacuole and cytoplasm is always zero.

In the original OnGuard platform, the turgor pressure at each instant in time was assumed to arise from the osmotic pressure of the guard cell so that

$$P = RT(Q_T/V_T - C_{iso}) \quad (A1)$$

where V_T is the volume of the guard cell with the osmotic load Q_T under the prevailing pressure constraints of the cell wall and the surrounding epidermal or subsidiary cells, and R and T have their usual meanings (Appendix Table 1). In this formulation, C_{iso} defined the sum of the concentrations of all osmotically active solutes in the extracellular space, the apoplast, and the water potential of the apoplast and was assumed to be determined entirely by these solutes. Solving for V_T,

$$V_T = Q_T/(P/RT + C_{iso}). \quad (A2)$$

Evaporation from the leaf commonly has been envisaged to be driven by the water vapor gradient between the liquid-water interface within the leaf and the air outside, $\Delta w = w_{sat} - w_{air}$, where w_{sat} and w_{air} are the partial vapor pressures of water at saturation and in the air, respectively. Peak and Mott (2011) define a point *p* within the pathway for water vapor diffusion close to the guard cells between the evaporative surface and the air, thereby dividing Δw into two steps: The first step occurs between the evaporative surface and *p* with gradient $\Delta w_i (= w_{sat} - w_p)$, and the second occurs across the stomatal pore with gradient $\Delta w_s (= w_p - w_{air})$, where w_p is the partial vapor pressure of water at *p* (Figure 1).

To incorporate the vapor phase at point *p* within OnGuard2, we assume thermal equilibrium with the liquid phase water of the guard cell so that the water vapor content at point *p* is

$$RT/v_L \cdot \ln(w_p/w_{sat}) = P - cRT. \quad (A3)$$

Equation A3 is identical to Equation 4 of Peak and Mott (2011), where v_L is the molar volume of liquid water (~0.018 L/mol) and c is the concentration of osmotically active solute in the guard cell. Note that Peak and Mott (2011) define c without consideration of solute compartmentation or osmotically active solute in the apoplast. Now, we assign c_i to the solute within the guard cell ($= Q_T/V_T$) and define the osmotically active solute in the apoplast as C^o_{iso} so that osmotically active solute content effective in the guard cell $c = c_i - C^o_{iso}$. Substituting for c in Equation A3 and rearranging then yields

$$c_i = Q_T/V_T = P/RT + 1/v_L \cdot \ln(w_{sat}/w_p) + C^o_{iso} \quad (A4)$$

and solving for V_T gives

$$V_T = Q_T/(P/RT + 1/v_L \cdot \ln(w_{sat}/w_p) + C^o_{iso}). \quad (A5)$$

Comparing Equations A2 and A5, it is clear that C_{iso} may be redefined in Equation A2 as

$$C_{iso} = C^o_{iso} + 1/v_L \cdot \ln(w_{sat}/w_p) \quad (A6)$$

where C^o_{iso} defines the value of C_{iso} when $w_p = w_{sat}$, that is, when $1/v_L \cdot \ln(w_{sat}/w_p) = 0$. In other words, C^o_{iso} defines the osmotic potential of solute in the apoplast and $1/v_L \cdot \ln(w_{sat}/w_p)$ defines the osmotic potential arising from water vapor equilibration. Equations A2 and A6 thus yield the new relation of Equation 1a,b between cellular solute content, volume, and turgor and incorporate the contributions of apoplastic solute and of water potential in exchange with w_p.

Water Flux across the Guard Cell Plasma Membrane

In implementing Equation A2 in OnGuard, we assumed that water permeability across the guard cell plasma membrane normally does not limit V_T and that osmotic and turgor pressures balance within each iteration cycle. Water flux was therefore defined by

$$F_w = \Delta V_T/\Delta t \quad (A7)$$

where ΔV_T is the change in guard cell volume calculated over the time interval Δt. There are situations, however, in which water flux is restricted, such as may be associated with a reduced osmotic permeability through the regulation of plasma membrane aquaporins (Yang et al., 2006b; Chaumont and Tyerman, 2014; Grondin et al., 2015; Maurel et al., 2015). In these situations, the change in volume with each time interval will be proportional to the driving force generated during the interval. It can be shown that

$$F^r_w \Delta t = \Delta V^r_T = \Delta V_T(1\text{-}e^{-f\Delta t}) \quad (A8)$$

where F^r_w is the restricted water flux, ΔV^r_T is the consequent change in volume over the interval Δt, and *f* is a non-negative, pseudo-rate constant with units of s^{-1}. Equation A8 defines a first-order process and is consistent with trans-plasma membrane water flux that commonly approximates a simple exponential relaxation (Murai-Hatano and Kuwagata, 2007; Chaumont and Tyerman, 2014; Maurel et al., 2015).

To restrict water flux in OnGuard2, we interleave this relaxation with each iteration using ΔV^r_T to calculate a new value of V^n_T for iteration *n* so that

$$V^n_T = V^{n-1}_T + \Delta V^r_T. \quad (A9)$$

Thus, *f* adjusts the change in total volume calculated from the volume of Equation A5 to moderate the water flux and the corresponding volume change relative to V_T in each iteration. We use this new value, V^n_T, to calculate the variables for cytosolic and vacuolar volumes, solute concentrations, and turgor pressure. Finally, we implement ligand sensitivity to *f* as previously described for ion transport (Hills et al., 2012) so that *f* is scaled with one or more sets of Hill parameters assigned by the user to represent the dependence of F^r_w on ligands affecting plasma membrane water flux.

Implicit to V^n_T in Equation A9 is a residual osmotic potential across the plasma membrane. This residual adds to the osmotic potential generated by solute flux for balance in the next time interval. Thus, its iterative generation and carry-over accommodates an independent but slower relaxation in water flux. Clearly, when *f* is large, $\Delta V^r_T = \Delta V_T$ and V^n_T does not deviate from the value obtained with Equation A5. However, in practice, even very small values of *f*, which lead ΔV^r_T to depart appreciably from the balanced ΔV_T, do not have a substantial effect on the total volume in each increment because the iteration intervals are extremely short and therefore $V_T >> \Delta V_T$. An analysis of total volumes calculated with Equations A5 and A9 shows that, in a single, 10-ms interval with $\Delta V^r_T = 0.0001 \cdot \Delta V_T$, V^n_T deviates <2% from the value of

Appendix Table 1. OnGuard2 Parameter and Constant Definitions

Abbreviation	Definition
A_S	Stomatal pore area
A_W	Evaporative surface area scalar (=RWF)
c	Cellular solute concentration as defined by Peak and Mott
c_i	Total intracellular guard cell solute concentration ($=Q_T/V_T$)
C_{iso}	Total osmotic equivalence of the guard cell apoplast
C^o_{iso}	Osmotically active solute of the guard cell apoplast
D_S	Stomatal density of the leaf
D_W	Diffusion coefficient for water vapor in air at temperature T
d_e	Depth of mesophyll cell layer
d_S	Stomatal pore depth
δ	Voltage sensitivity coefficient
E	Transpiration from the whole leaf
E_S	Transpiration through a single stoma
E_X	Evaporation from the xylem within the unit leaf volume
E_K	Equilibrium voltage for K^+
F	Faraday's constant
f	Impedance coefficient for water flux
F_w	Plasma membrane water flux
F^r_w	Restricted plasma membrane water flux
g	Channel ensemble conductance at the prevailing voltage
g_{max}	Maximum channel ensemble conductance
g_s	Stomatal conductance ($=E/\Delta w_S$)
H_{vap}	Molar enthalpy of evaporation of water
I	Electrical current
J_W	Water flux per unit area through the stomatal pore
K	Mass transfer coefficient incorporating enthalpy of evaporation
p	Hypothetical site equilibrating water vapor with water in the guard cell wall
P	Turgor pressure
P_f	Water permeability
Q_T	Total osmotic content
R	Ideal gas constant
T	Temperature (°K) = (T_{leaf} + 273)
T_{leaf}	Leaf temperature (°C)
T_{air}	Air temperature (°C)
Δt	Iteration time interval
V	Voltage
$V_{1/2}$	Voltage at which $g = 0.5 \cdot g_{max}$
V_F	Air volume fraction of the leaf
v_L	Molar volume of liquid water
V_S	Leaf volume per stoma
V_T	Guard cell volume
V^n_T	Restricted guard cell volume at time increment *n*
ΔV^r_T	Restricted guard cell volume change
w_{leaf}	Partial vapor pressure of water inside the leaf
w_p	Partial vapor pressure of water at *p*
w_{sat}	Vapor pressure of water at saturation
Δw	Vapor pressure difference between leaf and air ($=w_{leaf}-w_{air}$)
Δw_i	Vapor pressure difference in the leaf ($=w_p-w_{sat}$)
Δw_S	Vapor pressure difference across the stomatal pore ($=w_{air}-w_p$)
W_w	Osmotic gradient for water flux across the plasma membrane
z	Scaling factor relating g_s and A_s ($=D_wD_s/d_s$)

V_T. Averaged over a 24-h diurnal cycle with each of the OnGuard2 models described here, the analysis shows that V_T^n never deviates by more than 0.00005% of the mean V_T. Thus, the adjusted volume increment ΔV_T^r yields values for V_T^n that are a good approximation to Equation A5.

Scaling and Delivering Water to the Leaf and Water Vapor to p

To scale models from the single stoma to the whole leaf and to determine w_p and g_s, we assign each stoma an equal fraction of the underlying total intercellular air space within the leaf for gas exchange. The intercellular volume, V_S, assigned to each stoma

$$V_S = d_e V_F / D_S \tag{A10}$$

where the values d_e and V_F are, respectively, the depth of the mesophyll cell layer and the volume fraction that is air space within the leaf, and D_S is the stomatal density over the leaf surface. V_S is used to scale the quantity of water transpired by the whole leaf. Diffusion through the stomatal pore is defined by Fick's Law such that

$$J_W = \Delta w_S \cdot D_W / d_S \quad \text{and} \quad \Delta w_S = w_p\text{-}w_{air} \tag{A11a, b}$$

where J_W is the flux per unit area through the pore, d_S is the depth of the stomatal pore, and D_W is the diffusion coefficient for water vapor in air. The micro-macro link is achieved by scaling this flux per stoma to the whole leaf surface

$$E_S = J_W \cdot A_S, \quad \text{and} \quad E = E_S \cdot D_S \tag{A12a, b}$$

where E_S is the transpiration through the single stoma and A_S is the area of the stomatal pore. As noted previously, g_s is commonly derived from E and Δw assuming $\Delta w \approx \Delta w_S \approx \Delta w_{sat}$. We now calculate g_s explicitly in relation to diffusion through the stomatal pore. Thus, from Equations A11a,b and A12a,b

$$g_s = E / \Delta w_S = z \cdot A_S, \quad \text{and} \quad z = D_w D_s / d_s. \tag{A13a, b}$$

OnGuard2 also provides g_s calculated in the conventional manner using Δw ($=w_{sat} - w_{air}$).

Finally, to complete the micro-macro link and Equations A5 and A6, we sought a mechanistic resolution of w_p. Evaporation within the leaf is a complex function of leaf temperature, T_{leaf}, water delivery through the xylem and transfer across the xylem parenchymal cells (Sack and Holbrook, 2006; Rockwell et al., 2014). To a first approximation, water delivery replaces the water transferred to the vapor phase and water lost via diffusion through the stomatal pore. Water transfer to the vapor phase from the xylem, E_X, may be represented by the relation

$$E_X = K \cdot T_{leaf} \cdot \Delta w_i = K \cdot T_{leaf} \left(w_{sat}\text{-}w_p \right) \tag{A14}$$

where K is a mass transfer coefficient that incorporates the molar enthalpy of evaporation. In the past, it has commonly been assumed that $w_p \approx w_{sat}$ that is $\Delta w_i \approx 0$. We calculate w_p, noting that the rate at which water vapor diffuses out through the stomatal pore generally must be balanced by the rate of evaporation from the internal leaf surfaces. The internal evaporative surface is recognized to be much greater than the area of the xylem (Sack and Holbrook, 2006; Rockwell et al., 2014). Adding a scaling factor for the evaporative surface area A_W gives the total evaporation rate

$$E = E_X \cdot A_W, \tag{A15}$$

and working back through Equations A11 to A15 yields

$$w_p = (A_w / A_S + z \cdot w_{air} / K \cdot T_{leaf}) / (A_w / A_S + z / K \cdot T_{leaf}) \tag{A16}$$

which can be sought numerically with each value of A_S. A_W is thought to vary substantially with hydraulic conductance through the xylem (Rockwell et al., 2014). This scalar therefore becomes a user-defined parameter, the RWF, that encapsulates water delivery to, and its conductance within, the leaf and, hence, any water stress arising through its restriction. In effect, for $A_w >> A_S$, $w_p \approx w_{sat}$ and for $A_w << A_S$, $w_p \approx w_{air}$.